2011

Determining the refractive index of liquids using a modified Michelson interferometer

Satyanarayana Rao Kachiraju

DETERMINING THE REFRACTIVE INDEX OF LIQUIDS USING A MODIFIED MICHELSON INTERFEROMETER

by

SATYANARAYANA RAO KACHIRAJU

A THESIS

Submitted in partial fulfillment of the requirements
for the degree of Master of Science
in
The Department of Physics
to
The School of Graduate Studies
of
The University of Alabama in Huntsville

HUNTSVILLE, ALABAMA

2011

In presenting this thesis in partial fulfillment of the requirements for a master's degree from the University of Alabama in Huntsville, I agree that the Library of this University shall make it freely available for inspection. I further agree that permission for extensive copying for scholarly purposes may be granted by my advisor or, in his/her absence, by the Chair of the Department or the Dean of the School of Graduate Studies. It is also understood that due recognition shall be given to me and to the University of Alabama in Huntsville in any scholarly use which may be made of any material in this thesis.

_____ _____

(Student signature) (Date)

THESIS APPROVAL FORM

Submitted by Satyanarayana Rao Kachiraju in partial fulfillment of the requirements for the degree of Master of Science in Physics and accepted on behalf of the Faculty of the School of Graduate Studies by the thesis committee.

We, the undersigned members of the Graduate Faculty of The University of Alabama in Huntsville, certify that we have advised and/or supervised the candidate on the work described in this thesis. We further certify that we have reviewed the thesis manuscript and approve it in partial fulfillment of the requirements for the degree of Master of Science in Physics.

_____ Committee Chair
(Date)

_____

_____

_____

_____ Department Chair

_____ College Dean

_____ Graduate Dean

ABSTRACT
The School of Graduate Studies
The University of Alabama in Huntsville

Degree___Master of Science_____ College/Dept. _____Science/Physics_____
Name of Candidate_____Satyanarayana Rao Kachiraju_____
Title_____Determining the Refractive Index of Liquids using a Modified Michelson___
Interferometer_____

An accurate method for measuring the refractive indices of liquids is proposed and experimentally verified. The experimental setup was a modified Michelson interferometer employing a novel chamber that allowed the optical path length to be varied accurately. The main advantage of the modified interferometer is its simple experimental setup, which was built using inexpensive optical components that were available in the laboratory. Image processing software was used to record, analyze, and accurately count the interference fringes. This experiment allowed determining the refractive index of a given liquid to the precision the wavelength of the laser light used was known.

Abstract Approval: Committee Chair _____

Department Chair _____

Graduate Dean _____

ACKNOWLEDGMENTS

I must extent heartfelt thanks to a number of people for their involvement in the development of this thesis. First and foremost, credit goes to my advisor, Dr. Don Gregory, and I would like to thank him for his support throughout this work and his guidance in every stage of this work. Without his guidance this thesis would not have been possible. I would also like to thank the other members of my committee, Dr. Mohan Sanghadhasa and Dr. Lingze Duan, for their insightful suggestions regarding my work. Their advice has helped me produce a quality thesis.

I would like to offer my sincere thanks to the Physics Department for teaching assistantship financial support throughout my master's research. Finally, I would like to thank my parents, family, and friends for their support and encouragement during the pursuit of this degree.

TABLE OF CONTENTS

Page

LIST OF FIGURES

LIST OF TABLES

LIST OF ABBREVIATIONS AND ACRONYMS

MI	Michelson interferometer
DPOCR	Analog differential phase detection in optical coherence reflectometer
FWHM	Full width half maximum
SWLI	Scanning white light interferometer
DPC-OCT	Differential phase-contrast optical coherence tomography
DPC-OCM	Differential phase-contrast optical coherence microscopy
SDPM	Spectral domain phase microscopy
SD-OCPM	Spectral domain optical coherence phase microscopy
SLD	Super luminescent diode

LIST OF SYMBOLS

n	index of refraction
c	speed of light
T	Time delay
λ	Wavelength
Δl	Optical path difference
V	Normalized intensity
R	Reflectivity
E	Input electric field
E_0	Beam amplitude
$\Delta\Phi$	Phase difference
I_1	Intensity of the beam
I_2	Intensity of the beam
$I_{1/2}$	Intensity of the beam
B_1	Dispersion constant
B_2	Dispersion constant
B_1	Dispersion constant
B_1	Dispersion constant
C_1	Dispersion constant
C_2	Dispersion constant
C_3	Dispersion constant
C_4	Dispersion constant

CHAPTER 1

INTRODUCTION

The index of refraction, or the refractive index, is a basic optical property of materials. Light travels at different speeds in different media. In addition, light travels slower through any medium or material that is not a vacuum. The speed of light in a vacuum is constant and is commonly denoted by c. The index of refraction of a given medium, n, is defined as the ratio of the speed of light in vacuum, c, to the group velocity of light in the medium, v. This ratio is shown as follows:

$$n = \frac{c}{v}.$$

The index is also a measure of the amount of refraction that will occur when light passes from one medium to another. The goal of this project is to propose and experimentally verify an accurate method of measuring the refractive index of liquids. The method proposed in this thesis measures the refractive index to the accuracy that the wavelength of the light is known.

The accurate measurement of the refractive index is of great importance in many branches of physics and chemistry and in industrial applications. The precise

determination of the refractive index can give insight into the purity of the material. In many cases, the refractive index data cannot be found in reference books and must be measured as needed. This is why it is useful to determine the refractive index with maximum accuracy and minimum effort and cost. The small differences in the refractive indices of various solutions are also very significant. There are various methods to determine the refractive index of liquids. Some of them are

- interferometric methods,
- minimum angle deviation and autocollimation methods, and
- Refractometer methods.

Each will be discussed in detail in Chapter 2.

Refractive index measurements are increasingly popular quality-assurance tools used in the food, beverage ingredients, and flavor industries. These measurements are used to determine the integrity and purity of raw materials that make up finished goods. The refractive index measurement is also used to determine the concentration of dissolved solids in a solution. For example, sugar and sweetener content is often the most critical and expensive component of food and beverage products. The refractive index measurement is used to determine the total sugar concentration in the product. Maintaining proper concentration ensures consistent quality and reduces cost, so products are routinely monitored from the raw material stage through the final stage of production. The refractive index measurements ensure good, consistent product quality and, more importantly, help to control production costs.

In addition, the accurate measurement of the refractive index of a liquid is of great importance in the oil and natural gas industry. Purities and impurities can affect the

performance, appearance, and capability of a solvent. The refractive index is very sensitive to differences in solvent compositions, so accurately determining the refractive index can give insight into the purity of the solvent. Therefore, the refractive index measurement is extremely useful in confirming the purity of liquid if the measurement can be made quickly and precisely.

The many uses and capabilities of refractive index measurements motivated this project. A simple and inexpensive experimental setup was designed and built for determining the refractive index experimentally. This experimental prototype can be further developed for application in various industries and operations.

The present investigation began by analyzing analog differential phase detection in an optical coherence reflectometer (Huang, Hsieh, and Chou). The differential-phase optical coherence reflectometer (DPOCR) was originally proposed to measure the suface profile of a given sample. While analyzing the DPOCR, an error was found in one of the plots of the published paper which eventually led to the present investigation. Figure 2.8 shows a DPOCR plot of the normalized intensity (V) vs. the optical path difference (Δl) (Huang, Hsieh, and Chou). Generally, when two waves interfere, the maximum interference intensity occurs at zero optical path difference, and minimum intensity occurs when the optical path difference equals half of the wavelength of the source light (λ). In Figure 2.8 of the paper, the maximum interference intensity was shown to occur at zero optical path difference, but the minimum interference intensity was predicted when the optical path difference equaled the wavelength (λ). There was clearly an error somewhere. The error was eventually found, but in the course of the investigation, another use for the technique was discovered.

The plot of the normalized intensity and optical path difference given in the paper was simulated using MATLAB software. While doing the simulation, a relationship was observed between the full width half maximum (FWHM) of that plot and the index of refraction. The DPOCR theory was easily modified to determine the refractive index of a liquid introduced into one of the arms of the interferometer. Two techniques, the FWHM method and a fringe-counting method, are proposed in this project to experimentally determine the refractive index of a given liquid with minimum effort and cost.

CHAPTER 2

BACKGROUND

The refractive index is an important optical parameter and extensive research has been done to measure it for liquids. The refractive indices of liquids have been measured using various methods and this chapter discusses some of them. Before examining the details of each method, this chapter discusses different kinds of Interferometric techniques used for measuring the refractive indices of liquids, gasses, and solids.

2.1 Interferometry

Interference occurs due to the superposition of two waves that originate from the same source and traverse different paths. Interferometry is a technique for diagnosing the properties of two or more waves by studying the pattern of interference created by their superposition. Interferometry is an important investigative technique in many fields like fiber optics, astronomy, engineering metrology, particle physics, and plasma physics.

Interferometry has numerous applications, among them measuring the refractive indices of any gas, liquid, or solid. The most commonly used interferometers to measure the refractive indices of gases are the Jamin interferometer and the Rayleigh interferometer. The Rayleigh interferometer employs two beams of light that are generated from a single source. They pass through two different cells that contain the

gases whose refractive index values are being compared. When it is required to measure the absolute value of the refractive index, one of the cells is evacuated, and the number of fringes moving past a given point in the far field is counted as the gas enters the empty cell. The advantage of the Rayleigh interferometer is that it is simple to construct, but the disadvantage is that the interference fringes must be viewed in high magnification. The Jamin interferometer is related to the Mach-Zehnder interferometer. In order to measure the refractive index of a sample, it must be placed in one arm of the interferometer; then the displacement it causes can be determined by simply counting the interference fringes. The Jamin interferometer allows very exact measurements of the refractive index of gases (Hariharan).

The Michelson interferometer (MI) is the most common configuration for optical interferometry. This interferometer was used in the famous Michelson-Morley experiment to show that the speed of light is a constant. Using this interferometer, Michelson conducted the first measurement of absolute distance. Another interferometer, the Sagnac interferometer, is used to detect angular velocity. In this architecture, two beams travel around the same circuit in opposite directions. When the whole interferometer, including the light source, is rotated with an angular velocity (ω), a fringe shift results. This fringe shift is caused by the introduction of a time delay (T) between two beams and is given by (Hariharan)

$$T=4\omega A\cos\theta/c^2 ,$$

where A is the area enclosed by the light path and ω is the angular velocity.

The use of electronics and digital computers has revolutionized interferometry. Digital computers are helpful when using fringe-counting interferometers for length

measurements. In addition, digital image acquisition and computer processing are useful in determining the interferometric phase directly from a set of interference images.

2.2 Interferometric Method

Interferometric measuring systems have been widely applied to accurately determine the refractive index of fluids. An optical fiber interferometric refractometer (Suhadolnik) is one of the instrument used to measure the refractive index of liquids. In the paper describing the device, a combined laser interferometer system consisting of a fiber-optic interferometer and a bulk optic interferometer is used. The measuring fiber-optic interferometer is based on the Mach-Zehnder configuration and the bulk interferometer is based on the Michelson interferometer. The fiber-optic Mach-Zehnder configuration measures the optical path in the liquid, and the bulk Michelson interferometer measures the sample displacement. Such a configuration is used for precise determination of the refractive indices of different liquids; however, the system is rather complicated and expensive.

The optical fiber interferometer is shown in Figure 2.1. A bulk optic beam splitter divides a He-Ne laser beam into two separate beams. Both beams are focused on the end faces of the optical fiber X-coupler and enter into the optical fiber. The beams then recombine in the fiber coupler. At the end of the fiber coupler, a photodiode is fixed in order to detect the interference fringes (Suhadolnik).

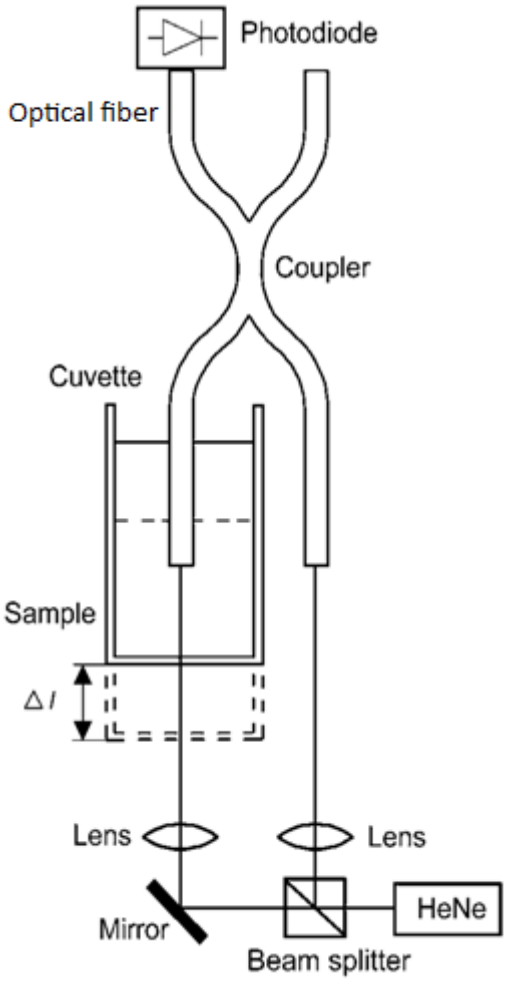

Figure 2.1 Schematic diagram of the fiber-optic Mach-Zehnder interferometer (Suhadolnik).

One arm of the laser input end of the optical fiber coupler is immersed in the cuvette filled with the liquid. The optical path length change is achieved by moving the sample cuvette for a predefined distance Δl. If the refractive index of the measured liquid is n_l, then the optical path change is $n_l \Delta l$. On the other hand, the path length change in air with the refractive index n_a due to the cuvette movement is $n_a \Delta l$. By combining both optical path lengths, the fringe count k_0 is calculated from the difference between the optical paths:

$$n_l \Delta l - n_a \Delta l = k_0 \lambda , \tag{2.1}$$

where λ denotes the laser wavelength. The cuvette displacement Δl is measured with the Michelson interferometer, and the optical path change in the moving arm of this interferometer is

$$2 n_a \Delta l = k_l \lambda , \tag{2.2}$$

where k_l is the fringe count of the Michelson interferometer. In both interferometers the He-Ne lasers are used at the wavelength λ = 632.8 nm. The sample liquid refractive index is finally calculated by combining Equations (2.1) and (2.2) (Suhadolnik).

$$n_l = n_a \left(\frac{2k_0}{k_l} + 1 \right) \tag{2.3}$$

The complete experimental setup is shown in Figure 2.2 (Suhadolnik), including both the Michelson and the Mach-Zehnder interferometer. The Michelson interferometer is used for the cuvette displacement measurement. The mirror is fixed on a vertical moving stage where the cuvette is also fixed. The vertical stage with a sample cuvette is moved by a dc motor. The problem with the experimental setup is the complicated nature of this method, which involves the combination of two different types of interferometers. The whole experimental setup is limited vertically by the height available above the optical bench.

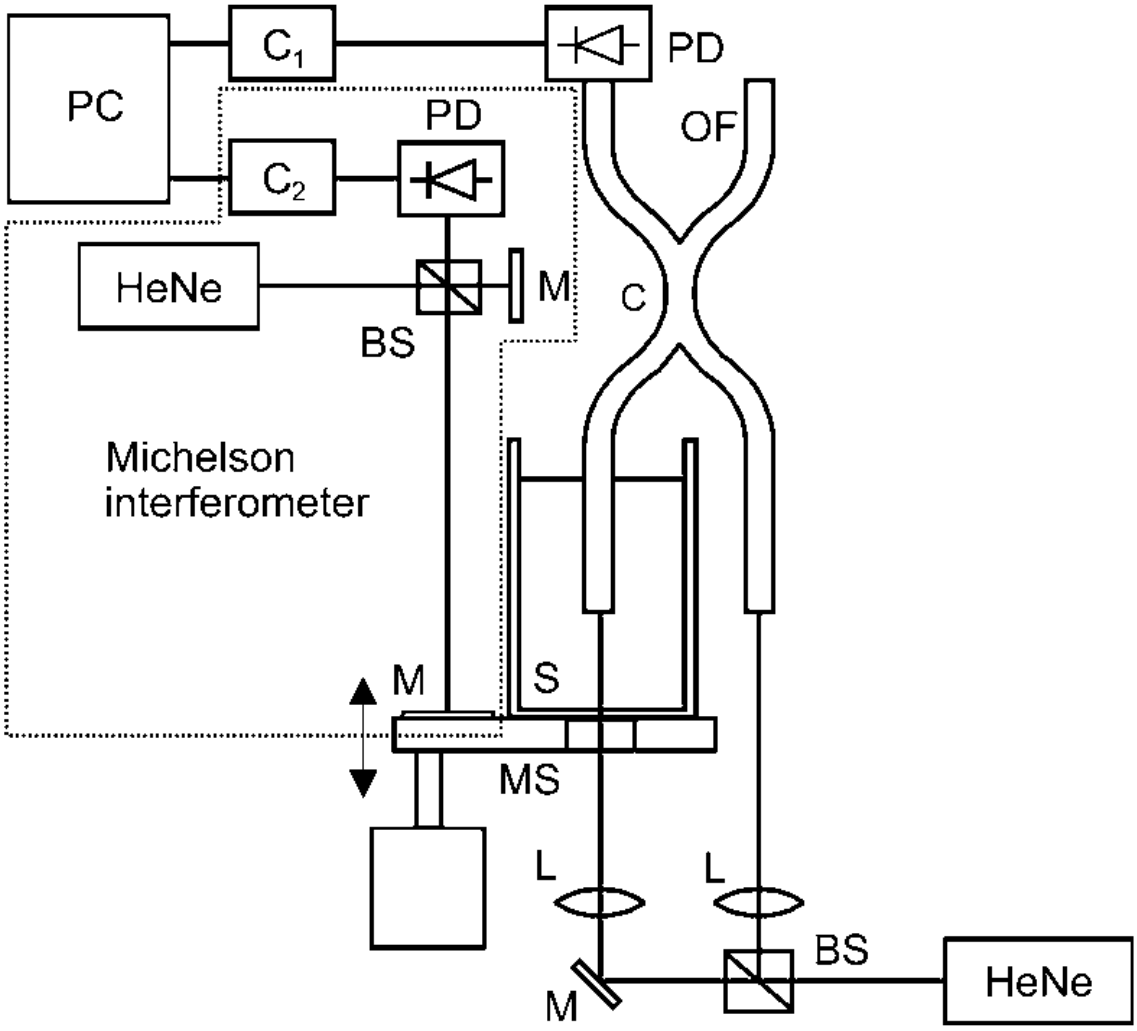

Figure 2.2 The experimental system consists of a fiber optic Mach-Zehnder interferometer and a Michelson interferometer
([C] Coupler; [OF] Optical fiber; [MS] Moving stage; [C_1] Counter 1; [C_2] Counter 2; [PD] Photodiode; [M] Mirror; [BS] Beam splitter; [S] Sample; [L] Lens; [PC] Computer; [HeNe] Laser) (Suhadolnik).

2.3 The Minimum Angle of Deviation Method

The minimum angle of deviation of a light beam that passes through a liquid contained in a triangular cell is often used to calculate the refractive index. In this method, the refractive index is determined by measuring the angle of minimum deviation for monochromatic light passing through a prism made of the material for which the refractive index is desired. In the case of liquids, a hollow prism with optically flat glass entrance and exit faces is filled with the liquid whose refractive index is being measured. Details are given below for a representative experiment (Grange, Stevenson, and Viskanta).

The hollow glass prism is filled with the liquid and securely fastened to the rotating table of an optical spectrometer capable of determining angles to within 20 arcsec. A 35mm-high, hollow glass prism with 50mm-wide faces and 60^{o} angles (obtained from Ealing Corp) was used to determine the refractive index of the liquid. A 2.5mW He-Ne laser at a 0.6328μm wavelength was used as the light source. One surface of the prism was illuminated with a collimated beam. The prism was then rotated, and the refracted beam observed through a telescope equipped with a crosshair. The point at which the beam changed direction identified the minimum angle of deviation. The position was recorded, and the same procedure repeated using the other surface of the prism. The difference between the two positions is twice the minimum angle of deviation. Figure 2.3 shows an experimental diagram illustrating the minimum angle of deviation, and Figure 2.4 shows the details used in deriving the minimum angle of deviation (Grange, Stevenson, and Viskanta).

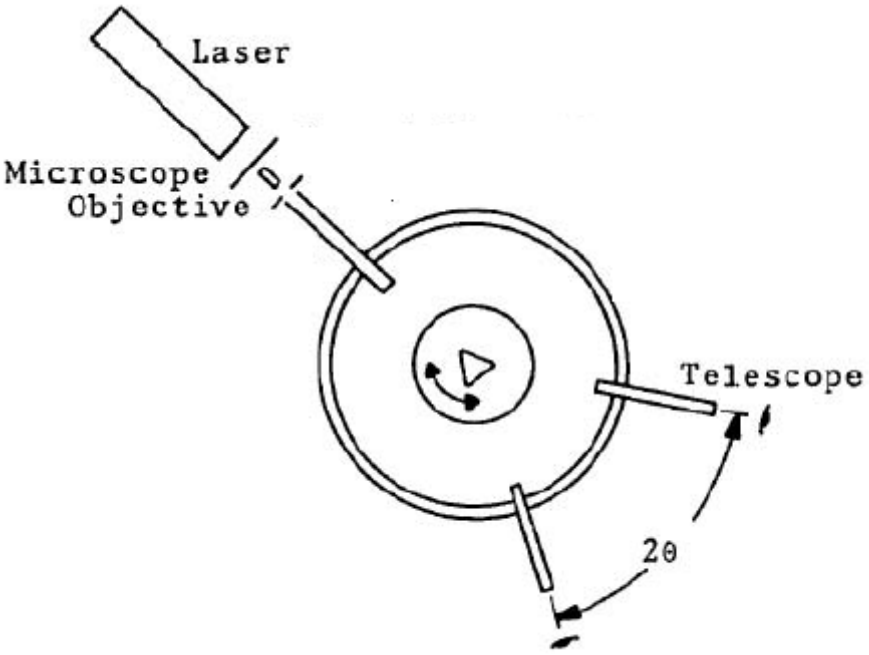

Figure 2.3 Schematic diagram of the minimum angle of deviation (Grange, Stevenson, and Viskanta).

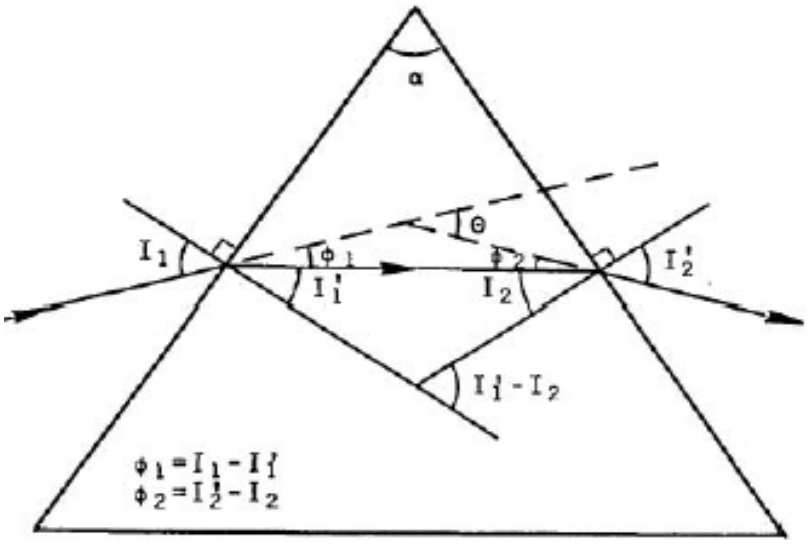

Figure 2.4 Details utilized in deriving the minimum angle of deviation (Grange, Stevenson, and Viskanta).

A collimated light beam of wavelength λ is incident at an angle I_1 on one face of a prism of included angle α. The angle of deviation θ is found to be a minimum if I_1 and I_2 are equal. A direct application of Snell's law yields Equation (2.4) for the refractive index of the liquid, n_l, at minimum deviation:

$$n_l = \sin[0.5(\alpha + \theta)] / \sin(0.5\alpha) . \qquad (2.4)$$

This method has been found to be a relatively simple and highly accurate for obtaining the refractive index of liquid solutions. However, a telescope must be used to locate the directional changes in the refracted beam. The probability of an error occurring when determining the angle θ is high (Grange, Stevenson, and Viskanta).

2.4 Refractometer Method

The automatic refractometer (Leung and Vandiver) is another of the methods which uses a liquid chamber to measure the refractive index. The refractive index measurement is performed with a refractometer. The sample chamber used to determine the refractive index of a transparent liquid was constructed with Plexiglas and glass slides. The base plate and two vertical walls of the chamber were made of Plexiglas. The other two walls of the chamber are thin microscope slides. One glass slide is perpendicular to the base plate, and the other glass slide was at an arbitrary angle of θ=13.8±0.1deg from the vertical axis, as shown in Figure 2.5 (Leung and Vandiver).

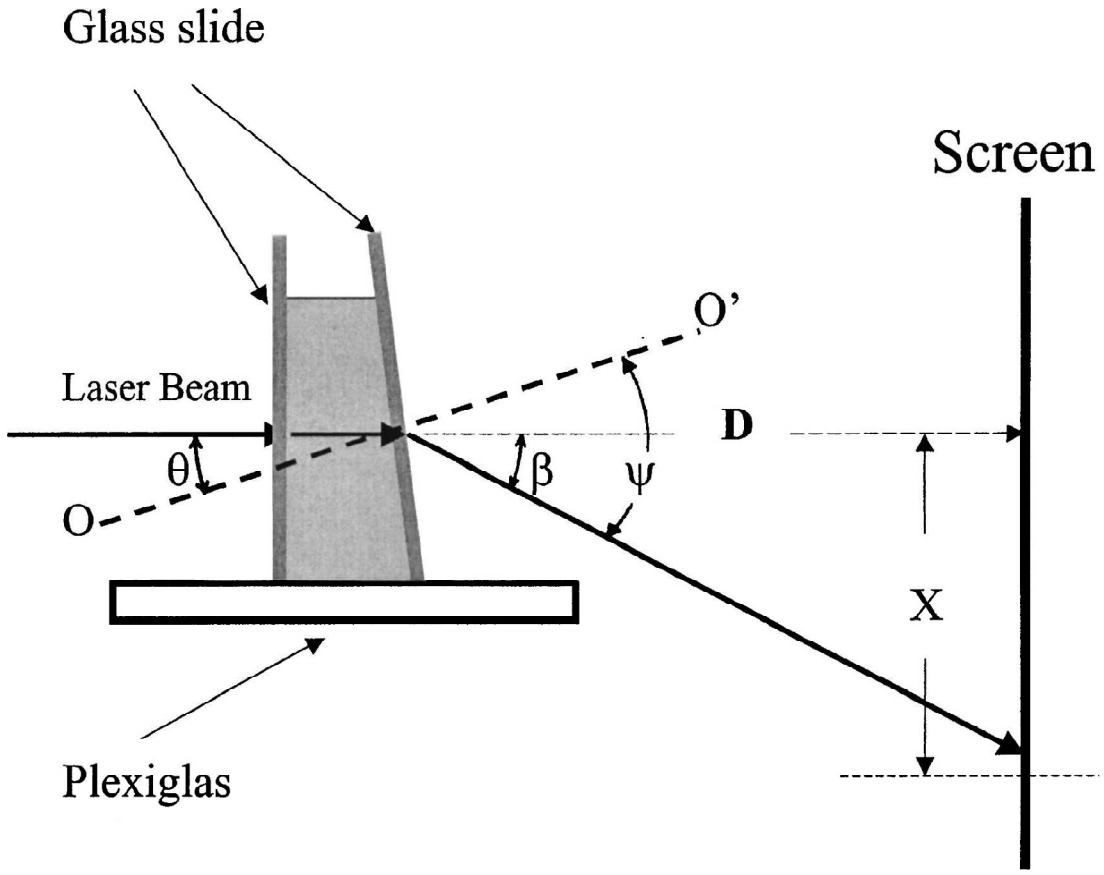

Figure 2.5 Refraction of the laser beam by the experimental chamber (Leung and Vandiver).

The sample liquid enters the chamber through an opening at the top. For the refractive index measurement, an ordinary He-Ne laser is used as the light source. The laser beam travels along the horizontal axis, illuminates the vertical glass slide of the sample chamber at normal incidence, passes through the liquid, and refracts at the liquid/glass/air interfaces.

Snell's law states that $n \sin\theta = n_{air} \sin\psi$, where n is the refractive index of the liquid, θ is the incident angle, and n_{air} the refractive index of air. The refraction by the thin glass slide is ignored. The refraction angle ψ is equal to $\theta+\beta$, where β is the angle

between the horizontal axis and the refracted beam exiting the experimental chamber. With n_{air} taken to be equal to unity, the refractive index of the liquid can be expressed as

$$n = \sin(\theta + \beta) / \sin\theta ,$$

The angle β can be determined by projecting the exiting beam onto a vertical screen placed at distance D from the point of exit. If the position of the light spot on the screen is located at a distance X below the horizontal axis, the angle β can be expressed as

$$\beta = \tan^{-1}(X / D) ,$$

then the refractive index of the liquid can be expressed as

$$n = \sin[\theta + \tan^{-1}(X / D)] / \sin\theta . \qquad (2.5)$$

The angle θ and distance D are constants in Equation (2.5). Then, n is a function of X only. A 1-D lateral photodetector (SiTek Electro Optics, model 1L10) of length 10 mm and width 2 mm was used to monitor the position of the refracted laser beam. It was mounted vertically on an x-y stage with attached micrometers. The liquid chamber used in this method has a specific configuration. One of the vertical walls of the chamber should be perpendicular to the base and the other vertical wall should be some θ angle to the base. The error in measuring θ affects the refractive index of liquid measurement. The refraction by the thin glass is ignored in this method. Figure 2.6 shows the experimental setup (Leung and Vandiver).

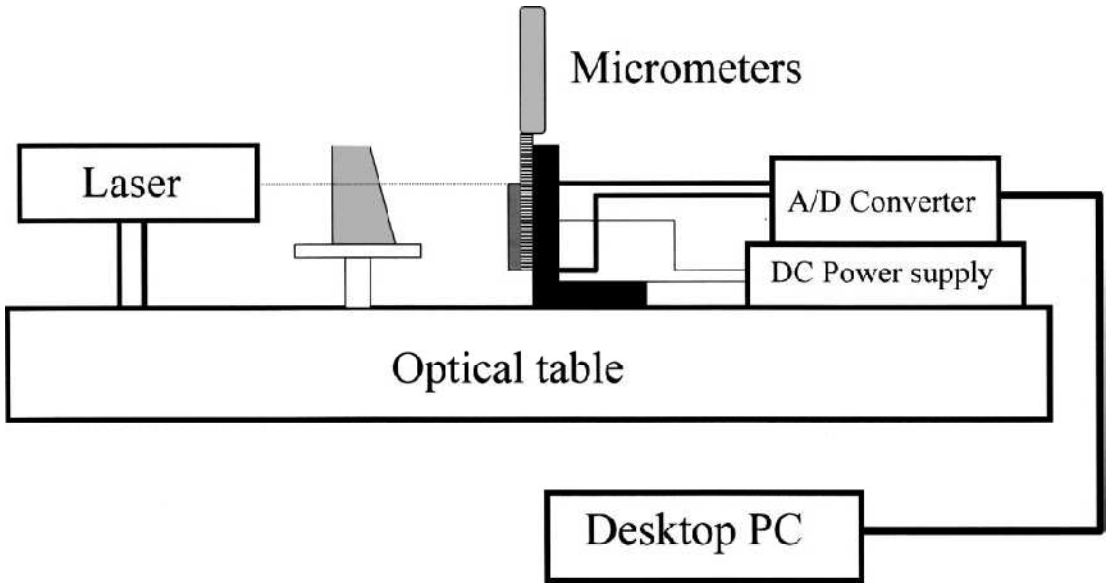

Figure 2.6 Experimental setup (Leung and Vandiver).

2.5 Surface Profilometry

Interferometric techniques can also be useful in measuring the surface roughness of samples. Interferometer-based surface profile measurements have been developed over many years (Kubota, Nara, and Yoshino; Lai and Yatagai). Most interferometers use monochromatic light sources and measure the displacement by obtaining the phase information through the process of decoding the phase difference using various analog methods. Hilbert transformation or autocorrelation algorithms are useful for decoding phase differences through numerical methods. However, this method is slow. Recently, low coherence surface profilometers have been developed which employ low coherence interferometers. This includes the scanning white light interferometer (SWLI) and optical tomography (OCT). Various phase-sensitive detection methods have been proposed, such as differential phase-contrast optical coherence tomography (DPC-OCT) and microscopy

(DPC-OCM), spectral-domain phase microscopy (SDPM), spectral-domain optical coherence phase microscopy (SD-OCPM), and phase-sensitive OCT using a Fourier domain mode-locked laser (FDML-PSOCT). Among them, the SD-OCPM and FDML-PSOCT, which utilize a wider spectral range of low coherence sources, have the capability to acquire axial displacement, and localize the surface profile with higher sensitivity compared to other methods using a narrower spectral range SLD (super luminescent diode) in a conventional OCT.

Differential-phase optical coherence reflectometry (Huang, Hsieh, and Chou) is one of the techniques used to measure the surface profile's fine structure at high sensitivity. In the DPOCR technique, a Michelson interferometer setup is used to detect the phase differences due to surface irregulrities. Figure 2.7 shows the schematic diagram of the DPOCR.

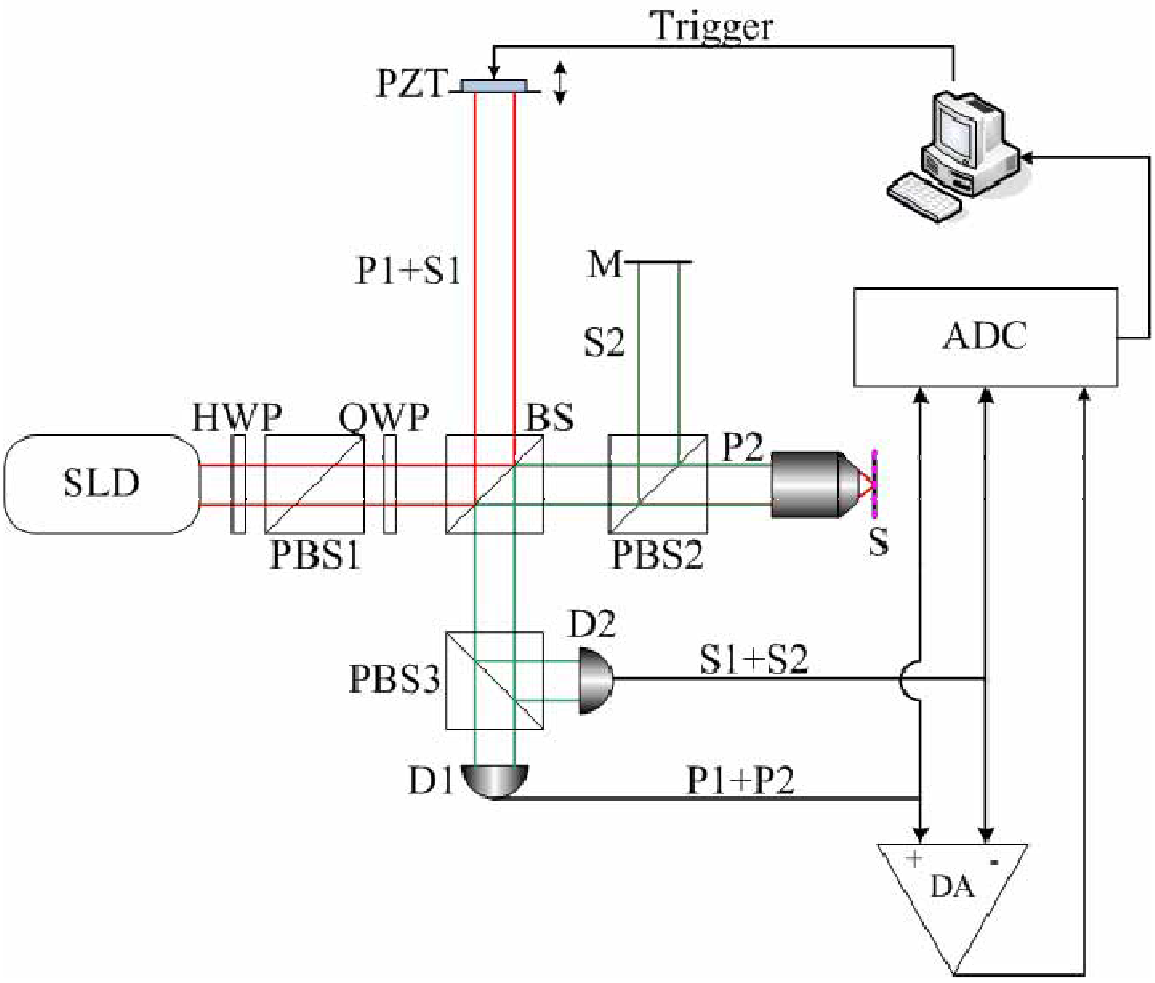

Figure 2.7 Schematic diagram of DPOCR
([HWP] half wave plate; [QWP] quarter wave plate; [BS] beam splitter; [PBS1, PBS2, PBS3] polarization beam splitters; [D1, D2] photo detectors; [DA] differential amplifier; [ADC] analog-to-digital converter; [S] sample; [M] mirror; [PZT] piezoelectric-supported mirror) (Huang, Hsieh, and Chou).

A super luminescent diode (SLD) with a central wavelength (λ) of 827nm was used as a low coherence light source. An analog differential phase decoding method was used to detect phase deviations, which are measured in real time in terms of amplitude variations, where three modulated heterodyne signals [P wave, S wave, and their

difference] are measured simultaneously. The differential signal due to the optical path difference created by displacing the mirror longitudinally with each step size of 28nm was measured using the PZT controlled precision stage. Figure 2.8 depicts one of the DPOCR plots that shows the optical path difference (Δl) and normalized intensity (V), defined as

$$V \propto \frac{\left(I_{diff}^{M}\right)^2 - \left(I_{V}^{M}\right)^2 - \left(I_{H}^{M}\right)^2}{2I_{V}^{M}I_{H}^{M}} \approx \cos(\Delta\phi). \qquad (2.6)$$

When analyzing the DPOCR, the authors (Huang, Hsieh and Chou) reported that the maximum intensity occurred when the optical path difference (Δl) was zero, and the minimum occurred when the optical path difference (Δl) was 827nm, which is equal to one wavelength. This is illustrated in Figure 2.8. In general, when two waves are superimposed, constructive interference occurs when the two waves are in phase, and destructive interference occurs when the two waves are 180^{o} out of phase. In other words, the constructive interference occurs when the optical path difference between two waves is zero, and destructive interference occurs when the optical path difference is an odd multiple of half of a wavelength, not a full wavelength. This was reason enough to investigate the model used, so a detailed step-by-step analysis was performed.

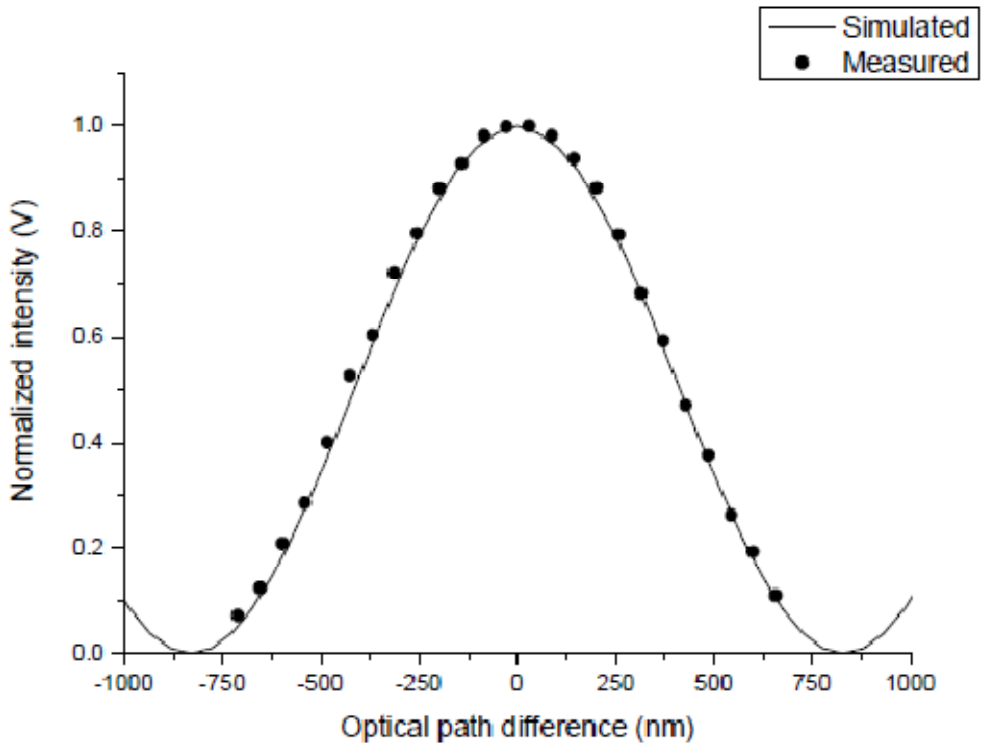

Figure 2.8 The measured data (dots) and computer simulation (solid lines) (Huang, Hsieh, and Chou).

The mathematical model which was used for simulations of the DPOCR was carefully examined and each and every equation in the model thoroughly verified. The model was reconstructed by writing the Jones vector of the circularly polarized input beam:

$$E = E_0 \begin{pmatrix} 1 \\ \pm i \end{pmatrix}, \tag{2.7}$$

where $E_0 = A_0(k)\exp[i(\omega t)]$ and $A_0(k)$ is the amplitude of the electric field and the wave number is $k=2\pi/\lambda$. In Equation (2.7), the electric field of a right-hand circular polarized

wave is decomposed into horizontal and vertical polarization components by beam splitters (BS). The reference beam and signal beams are given as

$$E_1 = \frac{1}{\sqrt{2}} E_0 \begin{pmatrix} 1 \\ -i \end{pmatrix} \tag{2.8}$$

and

$$E_2 = \frac{1}{\sqrt{2}} E_0 \begin{pmatrix} 1 \\ -i \end{pmatrix}, \tag{2.9}$$

respectively. In the reference arm, the PZT was modulated to generate a Doppler frequency shift, and the reference beam reflected by the PZT was decomposed into the P1 wave and S1 wave by PBS3. The signal beam was split by PBS2 into two orthogonal linearly polarized waves, denoted as the P2 wave and the S2 wave. The electric fields of P1, P2, S1 and S2 are given as

$$E_{P1} = \frac{\sqrt{R_1}}{2} E_0 \begin{pmatrix} 1 \\ 0 \end{pmatrix} \exp(-i2kl_{P1}), \tag{2.10}$$

$$E_{P2} = \frac{\sqrt{R_S}}{2} E_0 \begin{pmatrix} 1 \\ 0 \end{pmatrix} \exp(-i2kl_{P2}), \tag{2.11}$$

$$E_{S1} = \frac{\sqrt{R_1}}{2} E_0 \begin{pmatrix} 0 \\ -i \end{pmatrix} \exp(-i2kl_{S1}), \tag{2.12}$$

and

$$E_{S2} = \frac{\sqrt{R_M}}{2} E_0 \begin{pmatrix} 0 \\ -i \end{pmatrix} \exp(-i2kl_{S2}), \tag{2.13}$$

where R_1 is the reflectivity of the mirror mounted on the PZT, and R_S and R_M are the reflectivity of S and M, respectively. In addition, l_{P1} and l_{S1} are the optical path lengths of the P1 and S1 waves, and l_{P2} and l_{S2} are the optical path lengths of the P2 and S2 waves in the interferometer. Two P waves (P1+P2) and two S waves (S1+S2) are recombined and then separated by PBS3, resulting in P- and S- polarized optical heterodyned signals at photodetectors D1 and D2, respectively. The electric fields of the P waves and S waves are

$$E_P = \frac{1}{2} E_0 \left[\sqrt{R_1} \exp(-i2kl_{P1}) - \sqrt{R_s} \exp(-i2kl_{P2}) \right] \tag{2.14}$$

and

$$E_S = \frac{i}{2} E_0 \left[\sqrt{R_1} \exp(-i2kl_{S1}) - \sqrt{R_M} \exp(-i2kl_{S2}) \right]. \tag{2.15}$$

The intensities of P waves and S waves are given as

$$i_P = \gamma \left\langle E_P^* E_P \right\rangle_T , \tag{2.16}$$

$$i_P = \frac{\gamma A_0^2(k)}{4} \left[R_1 + R_S - 2\sqrt{R_1 R_S} \cos(2k\Delta l_P) \right], \tag{2.17}$$

and

$$i_S = \frac{\gamma A_0^2(k)}{4} \left[R_1 + R_M - 2\sqrt{R_1 R_M} \cos(2k\Delta l_S) \right], \tag{2.18}$$

where γ is the quantum efficiency of the photo detectors and $\Delta l_P = l_{p1} - l_{p2}$ while $\Delta l_S = l_{S1} - l_{S2}$.

For the current purposes, $\Delta l_P = \Delta l_S = \Delta l$, and the interference signals are integrated to obtain the peak values as

$$I_P^M \propto Max\{\frac{\gamma\sqrt{R_1 R_S}}{2}\exp\left[-\left(\frac{2\Delta l\sqrt{\ln 2}}{l_w}\right)^2\right]\cos(2k_0\Delta l_P)\} \tag{2.19}$$

and

$$I_S^M \propto Max\{\frac{\gamma\sqrt{R_1 R_S}}{2}\exp\left[-\left(\frac{2\Delta l\sqrt{\ln 2}}{l_w}\right)^2\right]\cos(2k_0\Delta l_S)\} \quad . \tag{2.20}$$

The differential signal when using a differential amplifier (DA) is

$$I_{diff} = \left|I_P - I_S\right| .$$

In Equation (2.21), the differential amplifier's output signal is related to the differential-phase (ΔΦ), which varies with the optical path difference of the P2 and S2 waves:

$$I_{diff}^M \propto Max\{\frac{\gamma\sqrt{R_1}}{2}\exp\left[-\left(\frac{2\Delta l\sqrt{\ln 2}}{l_w}\right)^2\right]\sqrt{R_S + R_M - 2\sqrt{R_1 R_M}\cos(\Delta\Phi)}\cos(wt-\theta)\} . \tag{2.21}$$

The normalized intensity (V) is defined as

$$V \propto \frac{\left(I_{diff}^M\right)^2 - \left(I_S^M\right)^2 - \left(I_P^M\right)^2}{2I_S^M I_P^M} \approx \cos(\Delta\phi) ,$$

which was also shown in Equation (2.6). Plotting the normalized intensity (V) as a function of the optical path length difference (Δl) gives the plot shown in Figure 2.9.

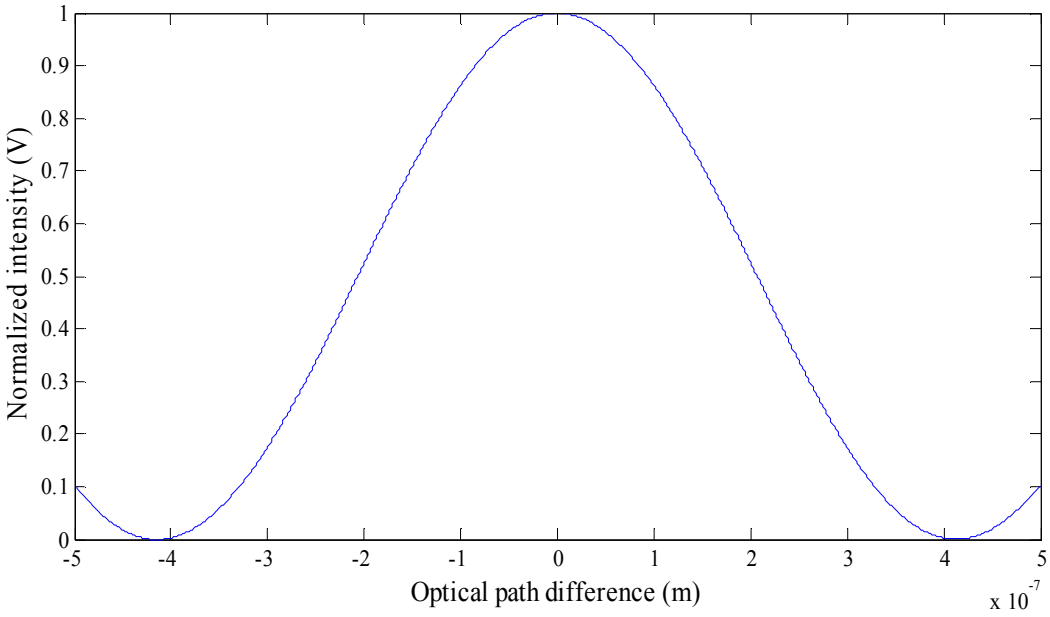

Figure 2.9 Computer simulated data using the mathematical model.

While conducting the simulations, it was observed that the refractive index of any liquid can also be obtained by doing some modifications to the DPOCR experiment. The FWHM of Figure 2.9 will change when a liquid cell is introduced into one of the arms of the DPOCR setup. A model was then developed to extract the refractive indices of liquids. A simple experimental setup of the Michelson interferometer was used to then measure the refractive index. The model is discussed in the next chapter.

CHAPTER 3

EXPERIMENTAL DESIGN

A Michelson interferometer was used in this experiment to measure the refractive index values. This chapter describes the experimental setup and the instruments developed to measure the refractive indices of selected liquids.

3.1 The Michelson Interferometer

Interferometers are basic optical tools often applied to precisely measure index of refraction, wavelength, and propagation distance. Figure 3.1 on the following page shows the Michelson interferometer setup.

In the basic Michelson interferometer, light from a source is divided into two beams by a beam splitter placed at a 45 degree angle to the beam. The transmitted beam travels to the movable mirror, where it is reflected back to the beam splitter. The returning beam is deflected at a 90 degree angle by the beam splitter and then strikes the detector. Next, the reflected beam travels to the fixed mirror, where it is reflected and passes straight through the beam splitter to reach the detector. The two beams that are created are then directed toward the detector. They interfere to produce fringes. The optical path difference between the rays that are reflected from the fixed mirror and the

movable mirror is Δd. The center of the screen is bright when the optical path difference is an integral number of wavelengths. The condition for yielding maximum intensity at the center of the screen is

$$2\Delta d = n\lambda \,, \tag{3.1}$$

where λ is wavelength, n is an integer, and Δd is the optical path difference.

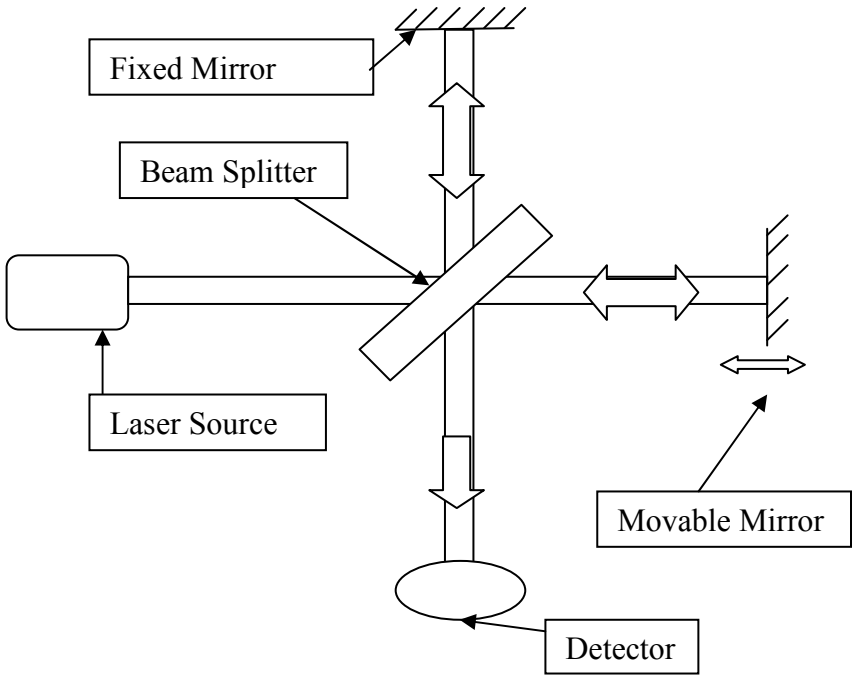

Figure 3.1 Schematic diagram of the Michelson interferometer.

3.2 Experimental Setup

The experimental setup is designed to determine the refractive index of any liquid. The setup is simple and easy to build when compared to the experimental setup required the DPOCR technique.

The experimental setup for this experiment is based on the Michelson interferometer. Figure 3.2 shows the experimental setup that was implemented. A floating optical bench supported the assembled set-up. The four legs of the optical bench were filled with air to isolate the optical bench from the ground. This reduced the effects of any vibrations on the interferometric measurements.

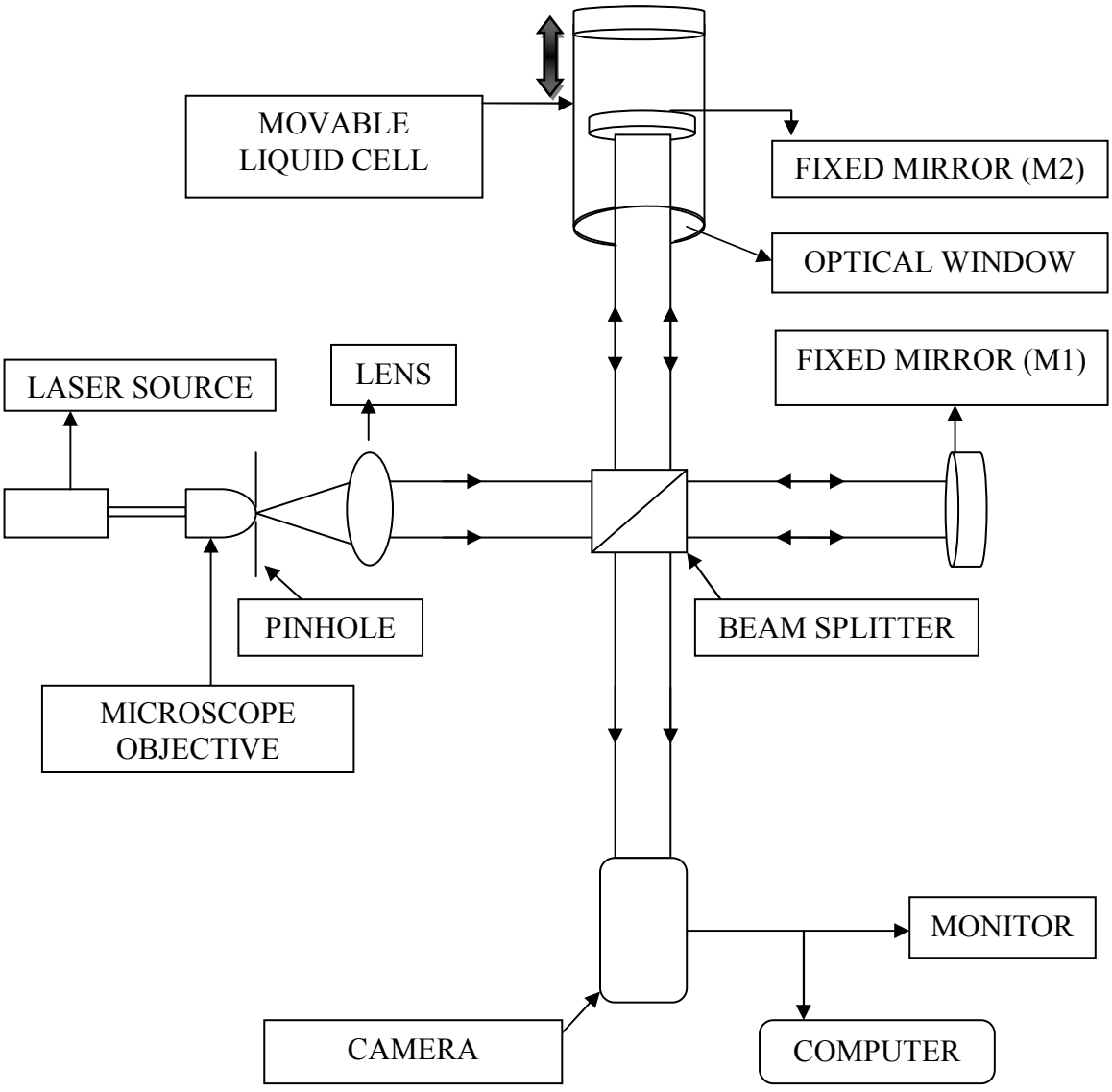

Figure 3.2 Schematic diagram of the experimental setup.

In this experiment, a 2.5mW He-Ne laser of 632.8nm wavelength was used as the light source. A microscope objective and a pinhole were used to expand the laser beam. The pinhole was adjusted so that the beam would be centered on the aperture of the collimating lens.

To produce a collimated beam, the following procedure was adopted. A plane parallel glass plate was inserted into the beam. As the light reflected from the two faces of the glass plate, the fringes that formed were observed. When the beam was convergent or divergent, straight parallel fringes were produced by adjusting the collimating lens back and forth . A uniform, fringe-free field was observed when the incident beam was collimated.

Once created, the collimated light beam was passed through a 50:50 cube beam splitter. The light beam was split into two beams that were perpendicular to each other, one of which propagated in the same direction as the original beam. The transmitted beam traveled to a fixed mirror (M1), where it was reflected back to the beam splitter. The returning beam was deflected at a 90 degree angle by the beam splitter and traveled to the detector. The reflected beam then entered the liquid cell, traveled through the liquid, and was reflected at the fixed mirror (M2) that was placed inside the liquid cell, again traversing through the beam splitter and to the detector. The liquid cell is described in Section 3.2.1. Section 3.2.2 explains the fixed mirror (M).

These beams were superposed and interference fringes were observed. A central bright fringe was observed when the optical path difference between these beams was zero. In addition, central bright and dark fringes were observed by changing the optical

path difference. Figure 3.3 shows the circular interference fringes observed on the television monitor.

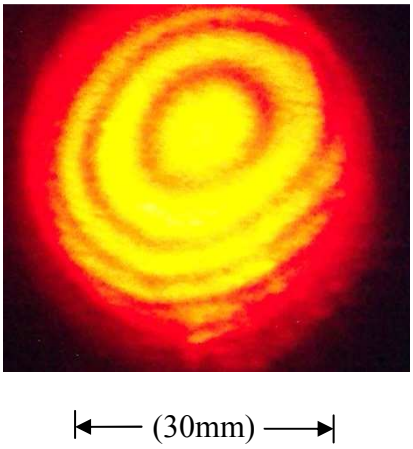

Figure 3.3 Circular interference fringes.

A camera was used to ensure the proper superposition of the light in order to record the interference pattern. A video monitor was connected to allow visualization of the camera's output. The superposition of the two beams was adjusted by observing the output on the monitor. Figure 3.4 shows the camera and the video monitor that were used in this experiment.

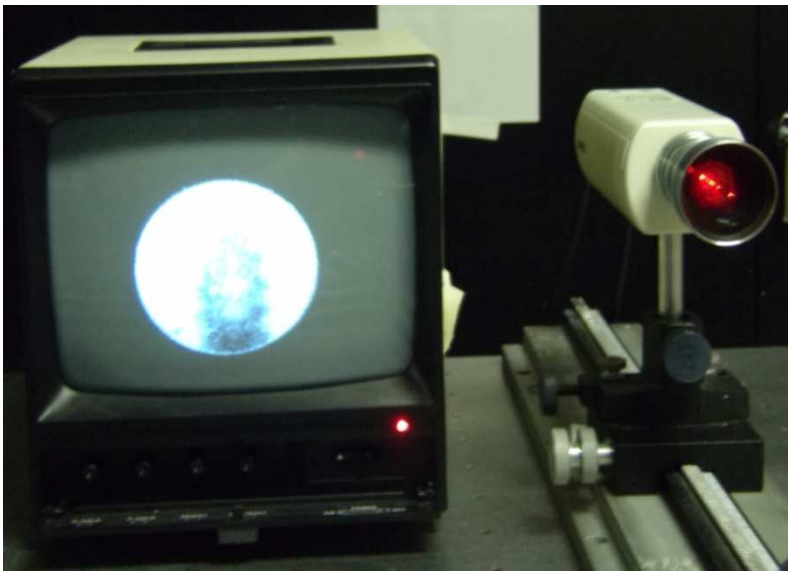

Figure 3.4 Camera and video monitor used to observe the fringes.

The camera output was also connected to a computer to record the interference intensity in a digital format. An image processing software program was used to record the interference intensity. This software program was written in LabVIEW and was modified based on the requirements of the experiment. Figure 3.5 shows the software home page.

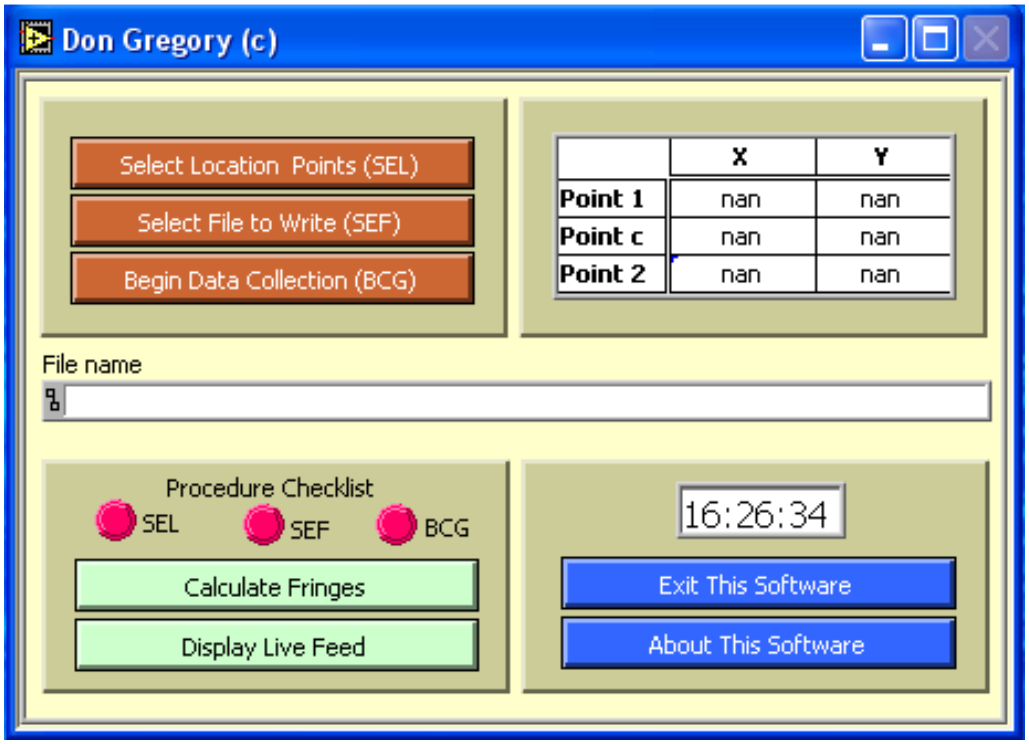

Figure 3.5 Software used to acquire and process the data.

The software performed a variety of functions. Like the video monitor, the software was able to produce a live picture of the fringe patterns. In addition, by using the Select Location Point (SEL) function, it was easy to choose any three location points of interest in the live picture. Intensities at these three points were acquired almost continuously, and were stored in a text file format. Data processing, noise reduction, and

fringe calculations could be done precisely. Figure 3.6 shows a sample of a fringe-counting calculation. In the figure, each dip represents one interference minimum.

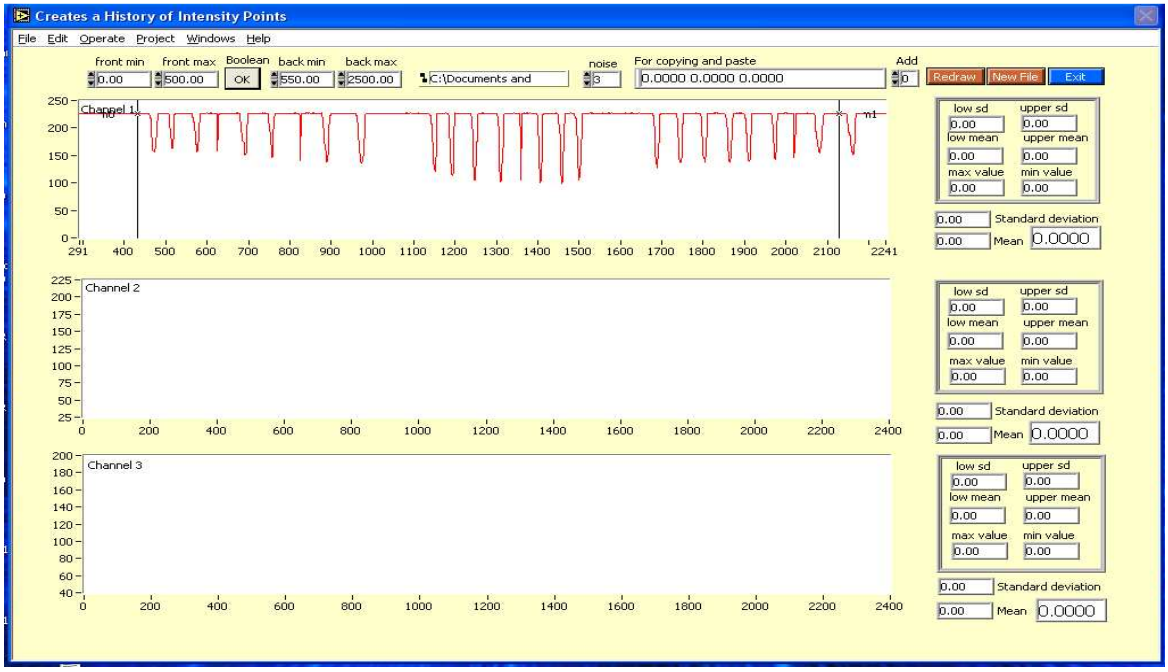

Figure 3.6 A sample screen showing a fringe-counting calculation.

3.2.1 The Liquid Cell

A custom-made liquid cell was introduced into one of the arms of the Michelson interferometer. This cell was cylindrically shaped with an optically flat quartz window at one end and a metal plate to cover the other end. Both of these ends were easily removed for cleaning. The cell had an opening in the top which allowed the mirror (M2) to be inserted into the liquid. The mirror was attached to a steel rod that could be fixed rigidly to the optical bench. Figure 3.7 shows a digital picture of the liquid cell.

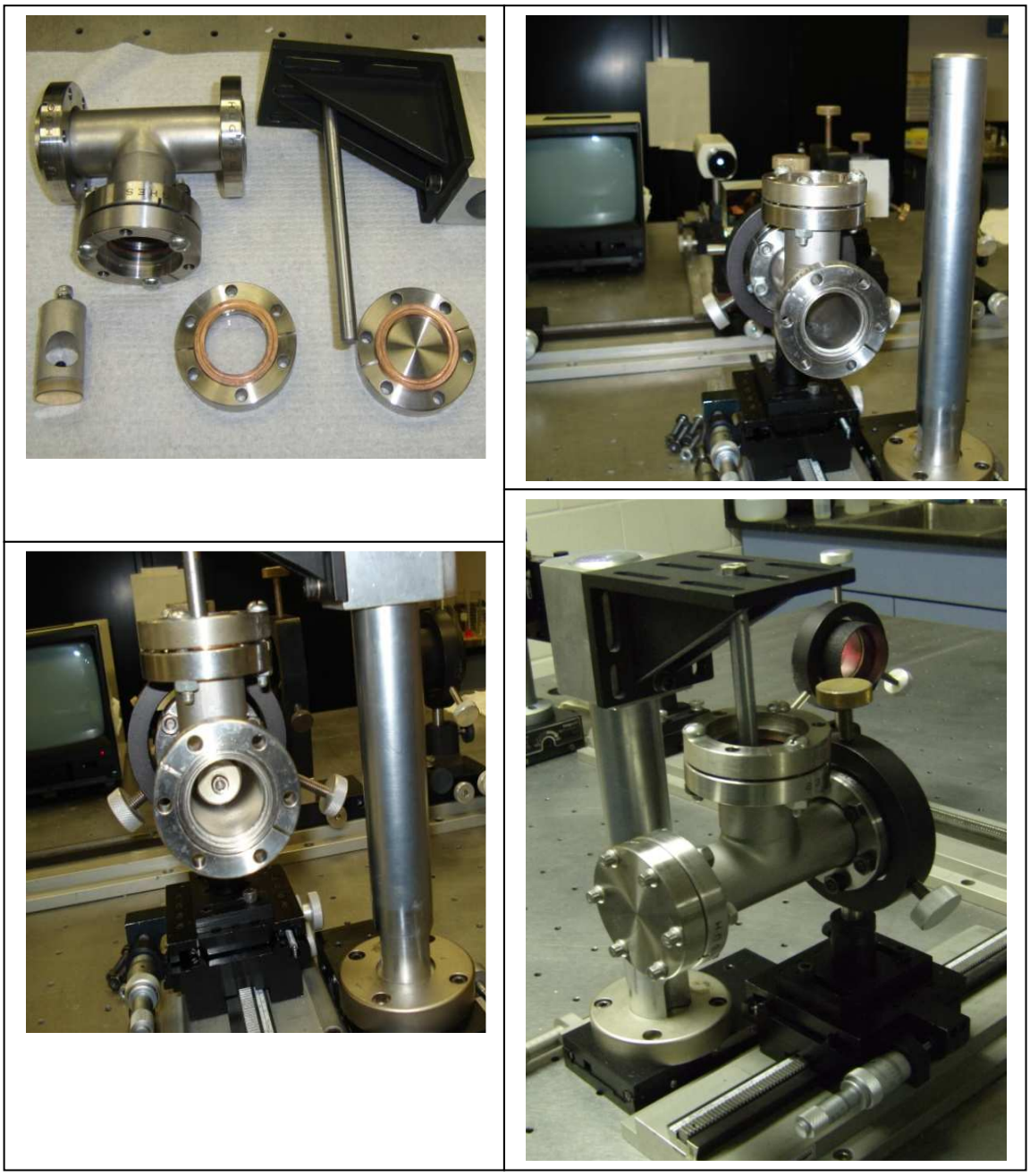

Figure 3.7 Digital picture of the liquid cell.

This cell played an important role in the process of measuring the refractive index of a given liquid. The liquid cell was filled with the liquid for which the refractive index was being measured. The liquid cell was mounted on a linear translation stage so that it

could be moved back and forth in order to change the amount of liquid between the quartz window and the fixed mirror (M2), a process that changed the optical path difference precisely. The liquid cell was placed on the linear translation stage in such a way that the entrance of the liquid cell and the mirror inside it were normal to the incident beam. Translating the cell while keeping the mirror fixed proved to be much more stable than translating the mirror.

3.2.2 Problems with the Mirror (M2)

This section describes the problems that resulted when the mirror, M2, was moved. Initially, M2 was mounted on a translating stage so that it could be moved back and forth inside the liquid cell. Then, M2 was moved inside the liquid cell using a micrometer to change the amount of the liquid between the quartz window and the mirror, a process that changed the optical path length precisely. But many real time problems occurred while moving M2, which affected the data. Some of the major problems were those associated with alignment and vibration.

M2 was attached to a custom made steel rod and inserted into the liquid cell. The mirror had three degrees of freedom when the cell was empty, but when the cell was filled with liquid, the mirror could not be controlled. While moving, M2 went out of alignment, which affected the interference fringe pattern. Another problem was vibration; while moving the mirror, vibrations occurred that also affected the fringes. Figure 3.8 shows a sample picture of an affected fringe pattern.

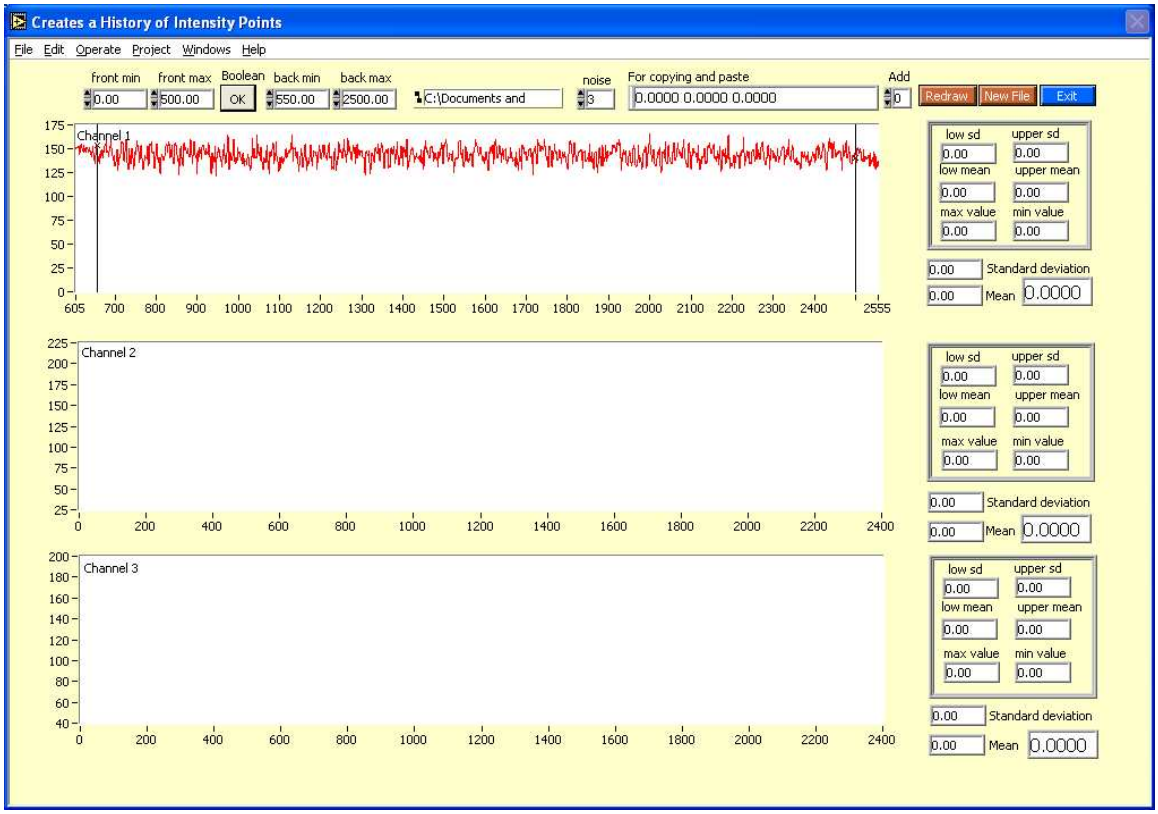

Figure 3.8 A sample screen of the affected fringe pattern.

Different experimental techniques were applied to reduce the alignment problem. In addition, different filters were written using MATLAB software for filtering the noise. These methods partially solved the problems but not completely. The problems were finally resolved by translating only the liquid cell while keeping the M2 mirror fixed rigidly to the optical bench.

3.2.3 The Motion Controller

Actuators play an important role in moving the translation stages. Different kinds of actuators with different resolutions were used in this experiment; in addition, both manual and motorized actuators were employed.

One of these manual actuators had an overall linear travel range of 13mm with a 0.0005mm (500nm) minimum increment; the other had an overall linear travel range of 2.5mm with a 0.0001mm (100nm) minimum increment. These actuators were essential in moving the translation stage and, thus, accurately changing the path length difference.

Besides the manual actuators, a stepper motor actuator (DVR014, Thorlabs) with a total linear travel range of 50mm was used. This actuator was specifically designed to be used with the linear translation stage LNR50. The stepper motor actuator was operated by a single channel stepper motor controller (BSC101, Thorlabs). This controller featured USB connectivity that provided easy plug-and-play computer operations. The driver was controlled by a computer using the Advanced Positioning System Technology (APT) software provided by Thorlabs.

Operating the motion controller was easy because of the many features and Graphical User Interfaces (GUIs) that were provided by the APT software. There were two methods for operating the motor actuator using the stepper controller: one was the jog mode and the other was the move mode. Two jog modes were available: single step and continuous. In single step mode, the motor moved by the step size specified in the step distance parameter. The smallest step size achieved was 50nm, meaning that, in each step, the translation stage was moved 50nm. In move mode, the motor moved the translation stage to a specified distance at a specified speed. The minimum speed that the translation stage could be moved was 0.0001mm/s. Figure 3.9 shows the stepper motor actuator with the motor controller.

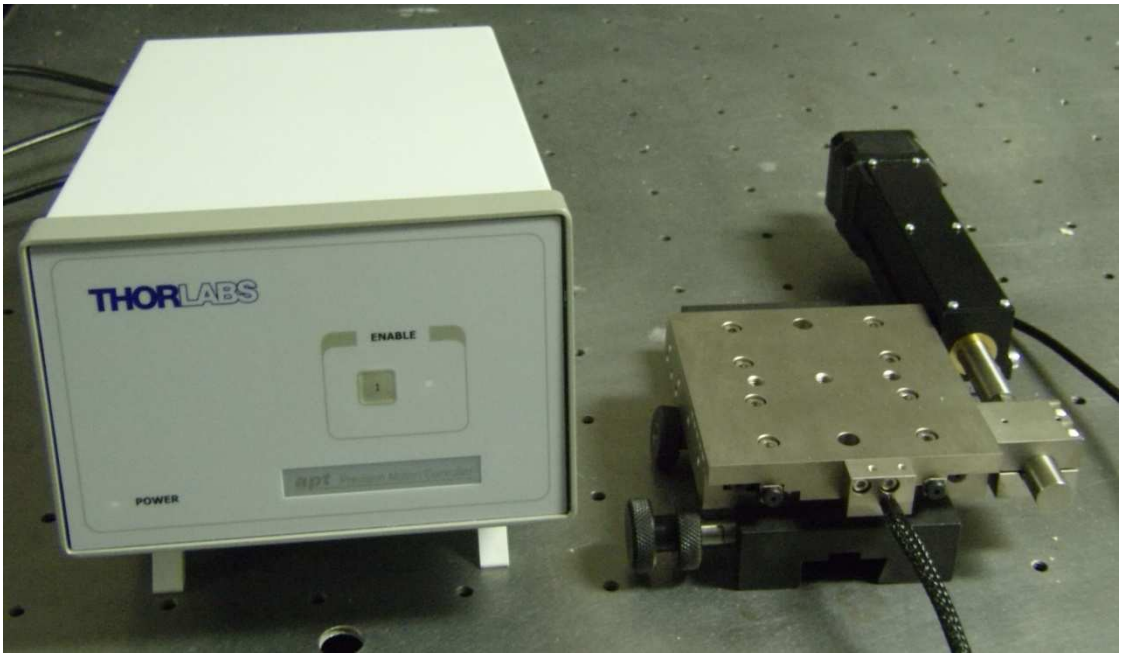

Figure 3.9 Stepper motor actuator with controller.

3.3 Data Acquisition

The laser beam was expanded by the microscopic objective and a well-collimated abeam traveling parallel to the optical bench was produced by the collimating lens. The beam splitter and mirrors had to be adjusted so that the beam retraced the same path after reflecting from the mirrors. The empty liquid cell was placed on the translation stage so that the quartz window was normal to the incident laser beam. The mirror (M2) was placed inside of the cell tube and adjusted to be normal to the incident beam. Both of the mirrors, M1 and M2, were adjused to obtain interference fringes. Then the liquid cell was filled with the liquid for which the refractive index was being measured. The optical path difference (Δl) was changed by moving the liquid cell at a predetermined speed to generate the dark and bright interference fringes, which were observed on the monitor

using the camera. The camera was focused to observe the central-order interference fringe. Intensities of the central-order fringes were recored in a text file format using the image processing software. The data was then analyzed to determine the refractive index of the liquid. Figure 3.10 shows the final experimental setup.

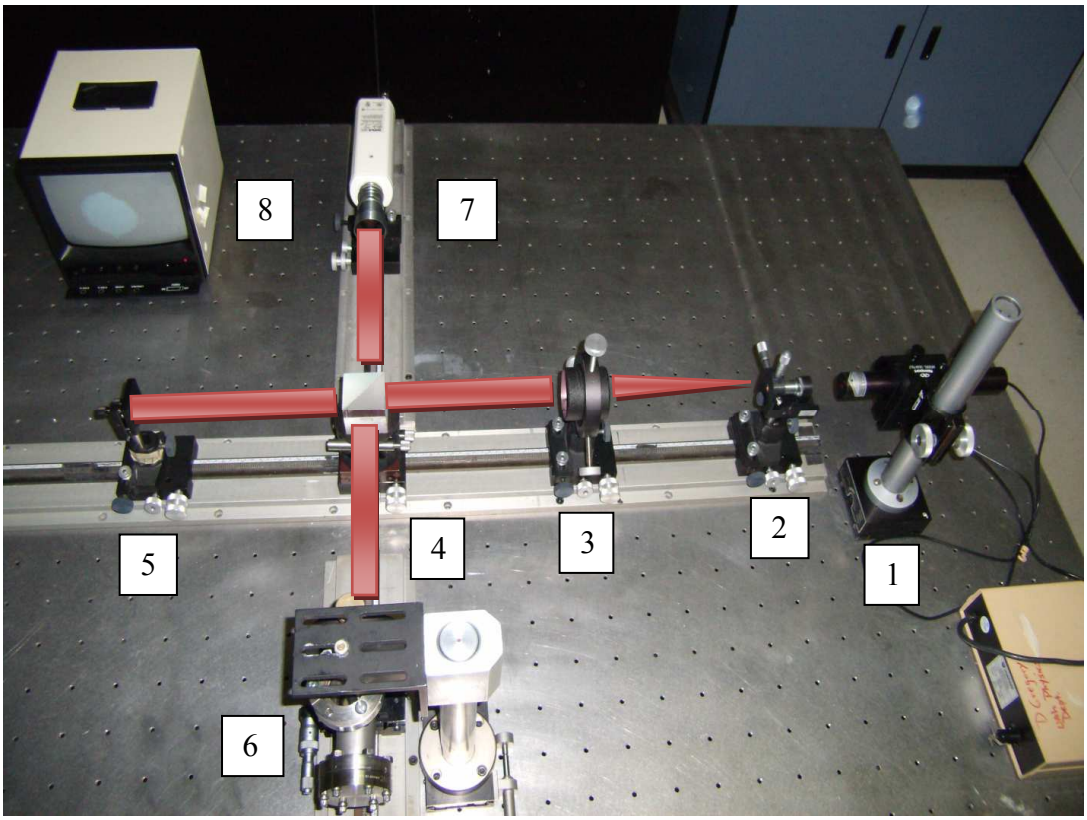

Figure 3.10 Photograph of the final experimental setup
([1] Laser Source; [2] Microscopic objective; [3] Collimating lens; [4] Beam splitter; [5] Fixed mirror (M1); [6] Liquid cell with fixed mirror (M2); [7] Camera; [8] Monitor).

CHAPTER 4

MODELING

This chapter discusses the physical models that were developed in this research and the two methods used in evaluating the experimental data: the full width half maximum (FWHM) method and the fringe-counting method.

4.1 Theory

Figure 4.1 shows the path lengths in the experimental setup.

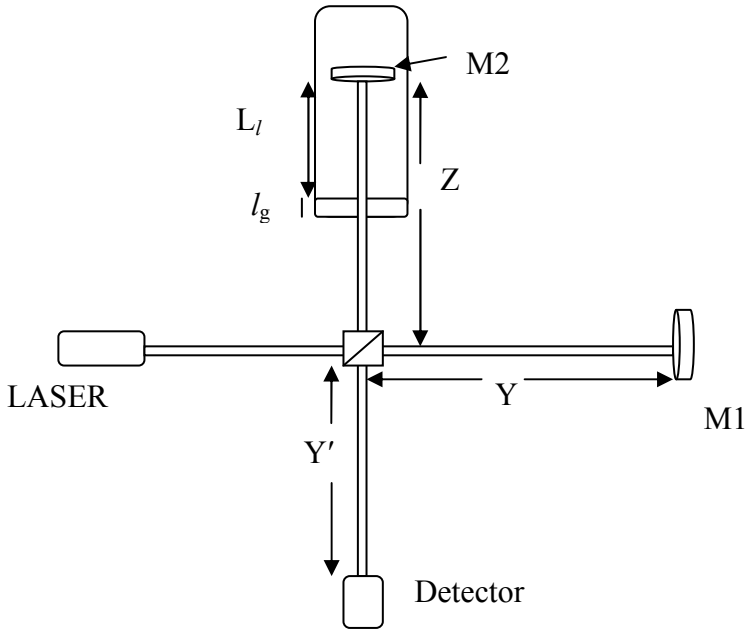

Figure 4.1 Experimental setup showing path lengths.

E_0 represents the amplitude of the electric field of the input laser beam. The beam amplitude was divided by a cube beam splitter and directed into the two arms of the interferometer as shown in Figure 3.2. The electric fields of the transmitted and reflected beams are written as

$$E_1 = E_{01}\exp(i2kY) \tag{4.1}$$

and

$$E_2 = E_{02}\exp(i2kZ), \tag{4.2}$$

where $k=2\pi/\lambda$ and Y and Z are the total path lengths that the light beams travel in the two arms. Both of the beams were reflected back at the fixed mirrors, M1 and M2; they then passed through the beam splitter and were superimposed at the detector. The total electric field of the output is given as

$$E_{out} = E_1 + E_2. \tag{4.3}$$

The irradiance of the output beam is

$$I = \varepsilon_0 c \left\langle E_{out}^2 \right\rangle_T, \tag{4.4}$$

By substituting Equation (4.3) into Equation (4.4) and expanding using the expression

$$E^2 = E \cdot E^*.$$

Then the irradiance can be expressed as

$$I = E_1 E_1^* + E_2 E_2^* + E_1 E_2^* + E_1^* E_2 . \quad (4.5)$$

Equation (4.5) can be written in a more convenient way by noting that

$$I_1 = \varepsilon_0 c \left\langle E_1^2 \right\rangle = \frac{E_{01}^2}{2} \quad (4.6)$$

and

$$I_2 = \varepsilon_0 c \left\langle E_2^2 \right\rangle = \frac{E_{02}^2}{2} . \quad (4.7)$$

The interference term $E_1 E_2^* + E_1^* E_2$ can be written as

$$I_{12} = 2\sqrt{I_1 I_2}\cos(\Delta\phi) . \quad (4.8)$$

By substituting Equations (4.6), (4.7), and (4.8), Equation (4.5) can be rewritten as

$$I = I_1 + I_2 + 2\sqrt{I_1 I_2}\cos(\Delta\phi) , \quad (4.9)$$

where $\Delta\phi = \frac{2\pi}{\lambda}(\Delta l)$ and Δl is the path length difference.

4.2 The Full Width Half Maximum (FWHM) Method

While reproducing the plot of normalized intensity (V) and optical path difference (Δl) (Figure 2.9), it was observed that the FWHM of the plot changed with the refractive index of the liquid used. A physical model was developed by modifying the DPOCR idea to determine the refractive index. Equations (2.19), (2.20), (2.21) and (2.6) were used for simulations in MATLAB. The phase difference ($\Delta\Phi$) in Equation (2.21) depends on the path length difference between P2 and S2 waves (see Figure 2.7). The expression for the

phase difference ($\Delta\Phi$) was developed by assuming that the liquid cell was introduced into the DPOCR setup shown in Figure 2.7. Based on Figure 4.1, the path lengths of the transmitted wave and the reflected wave are given as

$$l_T = 2Y+Y' \tag{4.10}$$

and

$$l_R = 2Z-2l_g-2L_l+2n_g l_g+2n_l L_l+Y' \ . \tag{4.11}$$

The path length difference is given as

$$\Delta l = l_R - l_T . \tag{4.12}$$

The phase difference between these two waves is given by

$$\Delta\Phi = k \cdot \Delta l ,$$

where $k=2\pi/\lambda$ and λ is the wavelength of the laser beam. By substituting Equations (4.10), (4.11), and (4.12), then $\Delta\Phi$ is written as

$$\Delta\Phi = (2kZ-2kl_g-2kL_l+2kn_g l_g+2kn_l L_l+kY') - (2kY+kY')$$

and

$$\Delta\Phi = 2k(Z-Y)+2kL_l(n_l-1)+2kl_g(n_g-1) \ ,$$

where l_g is the thickness of the quartz window, which is a constant, n_g is the refractive index of the quartz window, which is also a constant, and n_l is the wavelength-dependent

refractive index of the liquid. In addition, L_l is the thickness of the liquid between the mirror (M2) and the quartz window; the change in L_l provides the optical path length difference (Δl). Y and Z are the lengths of the arms; when they are equal, $\Delta\Phi$ becomes

$$\Delta\Phi = 2kL_l(n_l - 1) + 2kl_g(n_g - 1) \ . \qquad (4.13)$$

Equation (4.13) was substituted into Equation (2.21) to find the numerical values of n_l, n_g, and l_g as well as the information required to simulate a plot of the normalized intensity (V) and optical path difference (Δl). As expected, a significant difference was observed between the FWHM of the plot in Figure 2.9 and the FWHM of the plot shown below in Figure 4.2, which incorporates the index of refraction of the liquid.

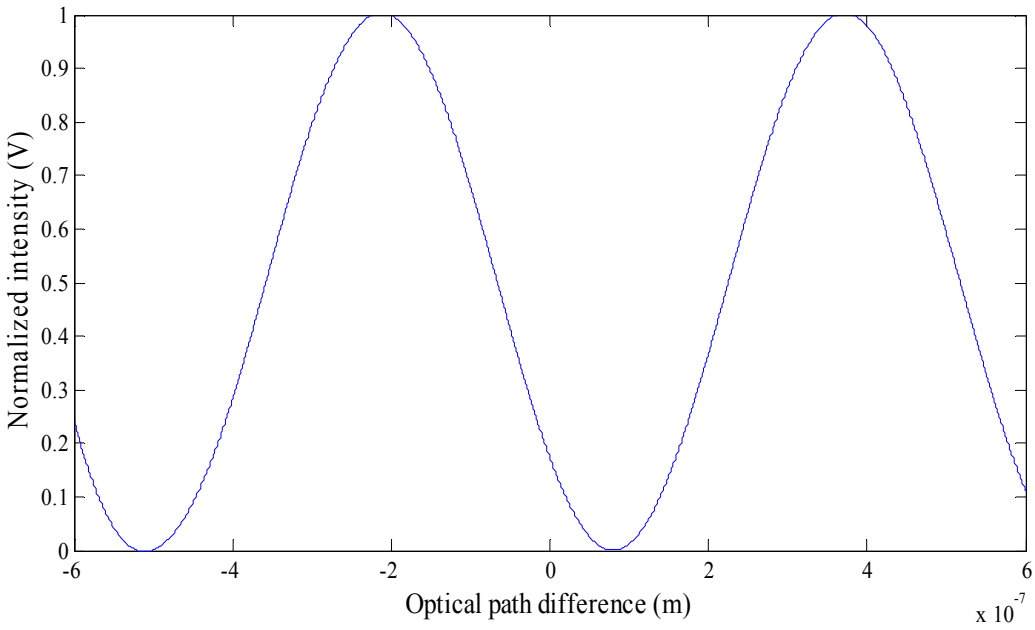

Figure 4.2 A simulated plot of the central order interference fringe intensity when the index of refraction of the liquid is considered.

Furthermore, Figure 4.3 also shows the effect of the refractive index of the liquid on the FWHM of the plot showing the normalized intensity (V) and optical path difference (Δl).

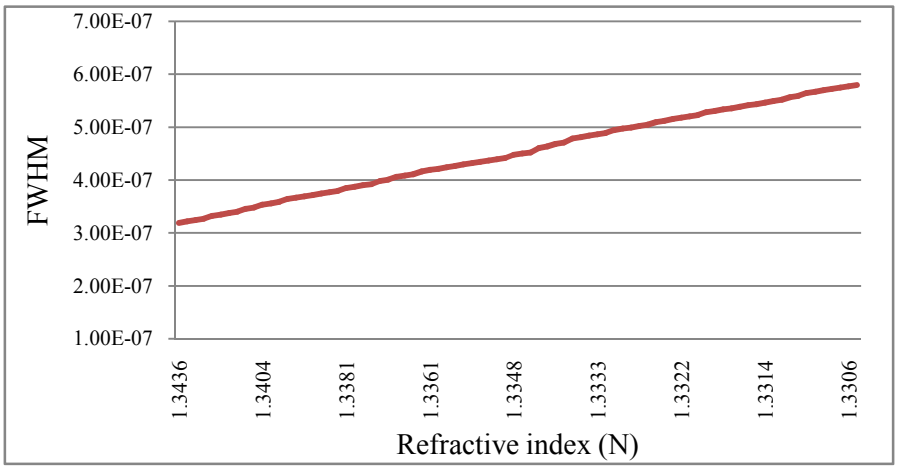

Figure 4.3 Refractive index of the liquid vs. the FWHM.

After the simulations were conducted, the refractive indices of various liquids were measured using the interferometer. The liquid cell was filled with liquid and aligned precisely to obtain the interference fringes. At the zero path length difference (Δl) of the two arms of the interferometer, the two beams were superposed perfectly onto each other to yield interference. A micrometer with 100nm minimum incremental motion was used to move the liquid, changing the path length difference. While moving the micrometer manually, interference intensities were recorded using the image processing software at each 100nm step. The optical path difference vs. normalized intensity is given in Figure 4.4. The FWHM of the plot in Figure 4.3 was obtained using a MATLAB program.

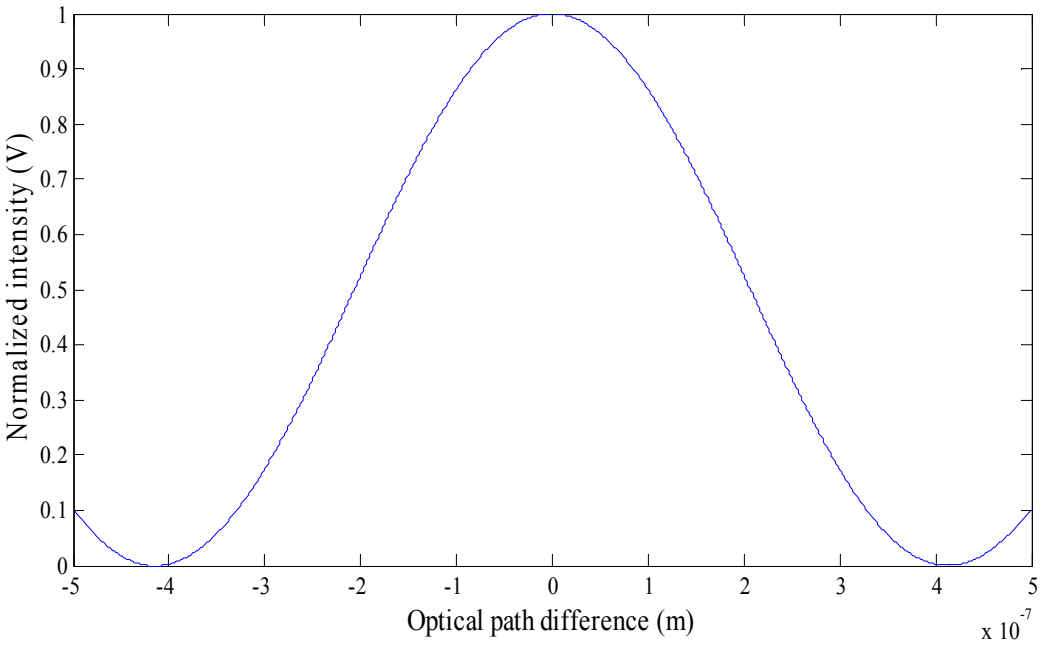

Figure 4.4 Plot showing the optical path difference ($\Delta l = L_l$) vs. normalized intensity.

Figure 4.4 shows that when constructive interference is involved, then the phase difference ($\Delta\Phi$) is zero. Therefore, Equation (4.13) becomes

$$0 = 2kL_l(n_l\text{-}1) + 2kl_g(n_g\text{-}1)\,.$$

Then the expression for the optical path difference, L_l, can be written as

$$L_l = \frac{-2kl_g(n_g - 1)}{2k(n_l - 1)} = L_{max}\,, \tag{4.14}$$

where L_{max} is the position of the micrometer at the interference intensity maximum. From Equation (4.9), which is the interference intensity equation, the interference intensity at the FWHM can be written as

$$I_{1/2} = I_1 + I_2 + 2\sqrt{I_1 I_2}\cos(\Delta\Phi_{1/2}) \ , \tag{4.15}$$

where $\Phi_{1/2}$ is the phase difference at the FWHM point and I_1 is the intensity of the transmitted beam. The value of I_1 was measured when the other arm of the interferometer was blocked. In contrast, I_2 represents the intensity of the reflected beam, and like I_1, it was measured when the interferometer's other arm was blocked. Finally, $I_{1/2}$ is the intensity output beam at the point of the FWHM. Therefore, the phase difference at the FWHM is written as

$$\Delta\Phi_{1/2} = \cos^{-1}\left(\frac{I_{1/2} - I_1 - I_2}{2\sqrt{I_1 I_2}}\right) \ .$$

Substituting the phase difference ($\Delta\Phi$) from Equation (4.13),

$$2kL_l(n_l - 1) + 2kl_g(n_g - 1) = \cos^{-1}\left(\frac{I_{1/2} - I_1 - I_2}{2\sqrt{I_1 I_2}}\right) \ ,$$

so

$$L_l = \frac{\cos^{-1}\left(\frac{I_{1/2} - I_1 - I_2}{2\sqrt{I_1 I_2}}\right) - 2kl_g(n_g - 1)}{2k(n_l - 1)} = L_{1/2} \ , \tag{4.16}$$

where $L_{1/2}$ is the position of the micrometer at the FWHM. So, the FWHM can be written in terms of the optical path length difference as $\frac{FWHM}{2}$, the path length difference at the FWHM minus the path length difference at maximum intensity. From Equations (4.14) and (4.16), the FWHM can be expressed as

$$\frac{\mathrm{FWHM}}{2} = (\mathrm{L}_{1/2} - \mathrm{L}_{\max}) = \frac{\cos^{-1}\left(\frac{\mathrm{I}_{1/2} - \mathrm{I}_1 - \mathrm{I}_2}{2\sqrt{\mathrm{I}_1\mathrm{I}_2}}\right) - 2\mathrm{k}l_{\mathrm{g}}(\mathrm{n}_{\mathrm{g}} - 1)}{2\mathrm{k}(\mathrm{n}_l - 1)} + \frac{2\mathrm{k}l_{\mathrm{g}}\ (\mathrm{n}_{\mathrm{g}} - 1)}{2\mathrm{k}(\mathrm{n}_l - 1)}$$

and can be restated as

$$\frac{\mathrm{FWHM}}{2} = \frac{\cos^{-1}\left(\frac{\mathrm{I}_{1/2} - \mathrm{I}_1 - \mathrm{I}_2}{2\sqrt{\mathrm{I}_1\mathrm{I}_2}}\right)}{2\mathrm{k}(\mathrm{n}_l - 1)},$$

then as

$$\mathrm{k}(\mathrm{n}_1 - 1) = \frac{\cos^{-1}\left(\frac{\mathrm{I}_{1/2} - \mathrm{I}_1 - \mathrm{I}_2}{2\sqrt{\mathrm{I}_1\mathrm{I}_2}}\right)}{\mathrm{FWHM}},$$

and finally the index of refraction can be expressed as

$$\mathrm{n}_l = \frac{\cos^{-1}\left(\frac{\mathrm{I}_{1/2} - \mathrm{I}_1 - \mathrm{I}_2}{2\sqrt{\mathrm{I}_1\mathrm{I}_2}}\right)}{\mathrm{k} \cdot (\mathrm{FWHM})} + 1\ . \qquad (4.17)$$

From Equation (4.17), the refractive index of a given liquid can be calculated from experimental data.

4.3 The Fringe-Counting Method

The mathematical equations for this model are derived from Equation (4.13). In this equation, the refractive index of the quartz window, n_g, is a constant for the wavelength of the source light. The thickness of the quartz window is l_g, which is also a constant. So, the second term is written as a constant (C). Therefore, the phase difference can be written as

$$\Delta\Phi = C + 2kL_l(n_l - 1) . \tag{4.18}$$

Let $\Delta\Phi = 2m\pi$ be the condition of the phase difference for the peak in irradiance. So Equation (4.18) is expressed as

$$2m\pi = C + 2kL_l(n_l - 1)$$

and

$$m = \frac{C}{2\pi} + \frac{kL_l(n_l - 1)}{\pi} ,$$

where $k=2\pi/\lambda$ and λ is the wavelength of the laser light.

$$m = C' + \frac{2\pi L_l(n_l - 1)}{\lambda\pi}$$

and

$$m = C' + \frac{2L_l(n_l - 1)}{\lambda}$$

Taking the derivative with respect to L_l

$$\frac{dm}{dL_l} = \frac{2}{\lambda}(n_l - 1) \ ,$$

and, thus, the index of refraction is expressed as

$$n_l = 1 + \frac{\lambda}{2}\frac{dm}{dL_l} \ . \tag{4.19}$$

The interference intensity data was recorded while moving the liquid cell to change the optical path difference a total of one mm. The data was recorded using the image processing software and the total number of fringes (dm) counted. Fringes were also counted manually for confirmation.

Both the motorized actuator and micrometer mentioned in Chapter 3 were used in this method to move the liquid cell while doing the experiment. While moving the liquid cell with the stepper motor actuator (DVR014, Thorlabs), great care had to be taken to move the cell smoothly. The minimum speed of the stepper motor is 0.0001mm/s. When the cell was moved using the minimum speed of the stepper motor, the detector was not able to see the evolution of the fringes separately. To record the intensities in a readable manner, the cell had to be moved with a speed slower than the minimum speed of the stepper motor.

To move the stepper motor at a slower speed, it was operated with a different option of the stepper motor controller (BSC101, Thorlabs). The stepper motor speed was reduced by choosing the continuous jog mode (described in Section 3.2.2) with zero time delay between the jogs. When the liquid cell was moved in this mode, the motor produced unwanted vibrations, which affected the experimental data. It was hard to count the total fringes using the corrupted data. Because of these problems, the stepper motor

actuator was replaced with a micrometer, which could be operated manually slow enough to observe the fringes clearly and record the data. A sample of the recorded data is shown in Figure 3.6.

Experimental data was analyzed using the image processing software for counting the total number of fringes (dm) passing a given point in 1mm of path length difference (dL_l). Refractive indices of the liquids were then calculated using Equation (4.19). The experimental results for a variety of liquids are discussed in the next chapter.

CHAPTER 5

RESULTS AND DISCUSSION

The purpose of this investigation was to develop a technique to precisely measure the refractive indices of liquids with little cost and minimum effort. The experimental results of the refractive index measurements of different liquids are presented and analyzed in this chapter.

5.1 Measuring the Refractive Index of Water

The refractive index of water was found experimentally using both the FWHM and fringe-counting methods. To simulate the FWHM for the water sample using the FWHM numerical model, Equation (2.21) was used to create a hypothetical plot of the normalized intensity VS optical path difference. The refractive indices of the quartz window, n_g, and water, n_l, were calculated using the Sellmeier equation, which is an empirical relationship between the refractive index and the wavelength for a particular medium. It can be written as

$$n^2(\lambda) = 1 + \frac{B_1\lambda^2}{\lambda^2 - C_1} + \frac{B_2\lambda^2}{\lambda^2 - C_2} + \frac{B_3\lambda^2}{\lambda^2 - C_3}\ , \tag{5.1}$$

where λ is the wavelength of the laser and B_1, B_2, B_3, C_1, C_2, and C_3 are the Sellmeier coefficients. The Sellmeier coefficients of quartz are shown in Table 5.1 while the Sellmeier coefficients of water are shown in Table 5.2.

Table 5.1 The Sellmeier coefficients of quartz (Cvi Melles Griot).

Coefficient	Value
B_1	0.696166300
B_2	0.407942600
B_3	0.897479400
C_1	$4.67914862 \times 10^{-3} \mu m^2$
C_2	$1.35120631 \times 10^{-2} \mu m^2$
C_3	$97.9340025\ \mu m^2$

Table 5.2 The Sellmeier coefficients of water (Daimon and Masumura).

Coefficient	Value
B_1	$5.684027565 \times 10^{-1}$
B_2	$1.726177391 \times 10^{-1}$
B_3	$2.086189578 \times 10^{-2}$
B_4	$1.130748688 \times 10^{-1}$
C_1	$5.101829712 \times 10^{-3}$
C_2	$1.821153936 \times 10^{-2}$
C_3	$2.620722293 \times 10^{-2}$
C_4	$1.069792721 \times 10^{1}$

The normalized intensity VS optical path difference for water was simulated and the FWHM was calculated to be 5.2168×10^{-7} m. The simulated plot is shown in Figure 5.1.

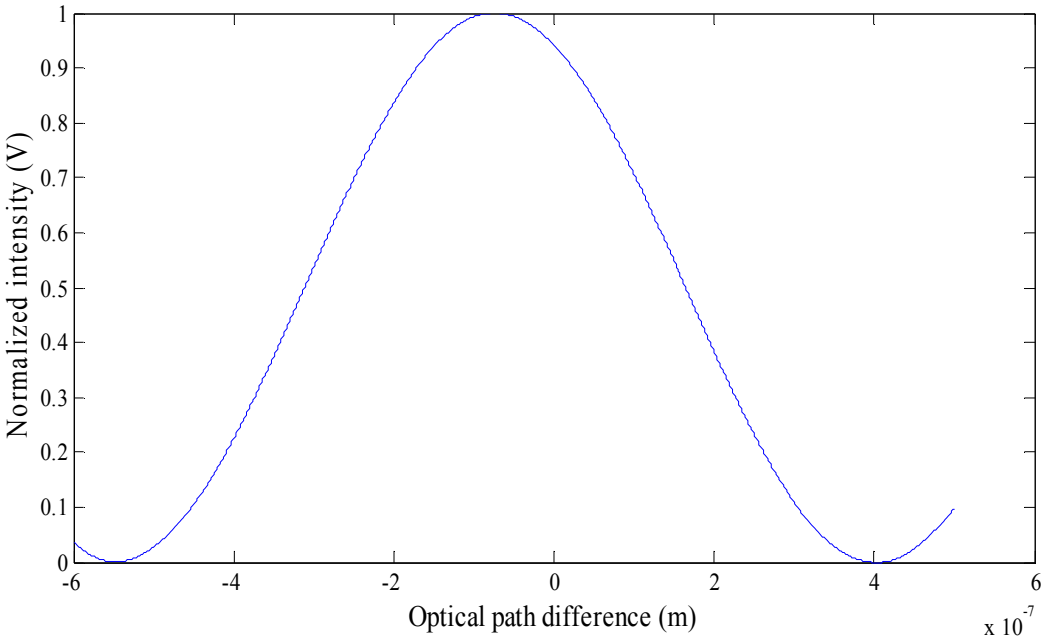

Figure 5.1 The simulated plot for the water sample.

The liquid cell was filled with distilled water to measure the refractive index experimentally. The mirrors, M1 and M2, were adjusted precisely to obtain the superposition of transmitted and reflected waves. Interference fringes were then observed on the video monitor. A manual micrometer with a minimum increment of 100nm was used to translate the liquid cell. A zero path length difference (Δl) was obtained by adjusting the micrometer manually. The interference intensities were recorded using the image processing software at every 100nm path length difference. In addition, the intensities of both the transmitted beam, I_1, and the reflected beam, I_2, were measured by

blocking alternate arms of the interferometer. The experimental data was plotted as the normalized intensity vs. the optical path length difference. Figure 5.2 shows the plot of the experimental data for the distilled water sample.

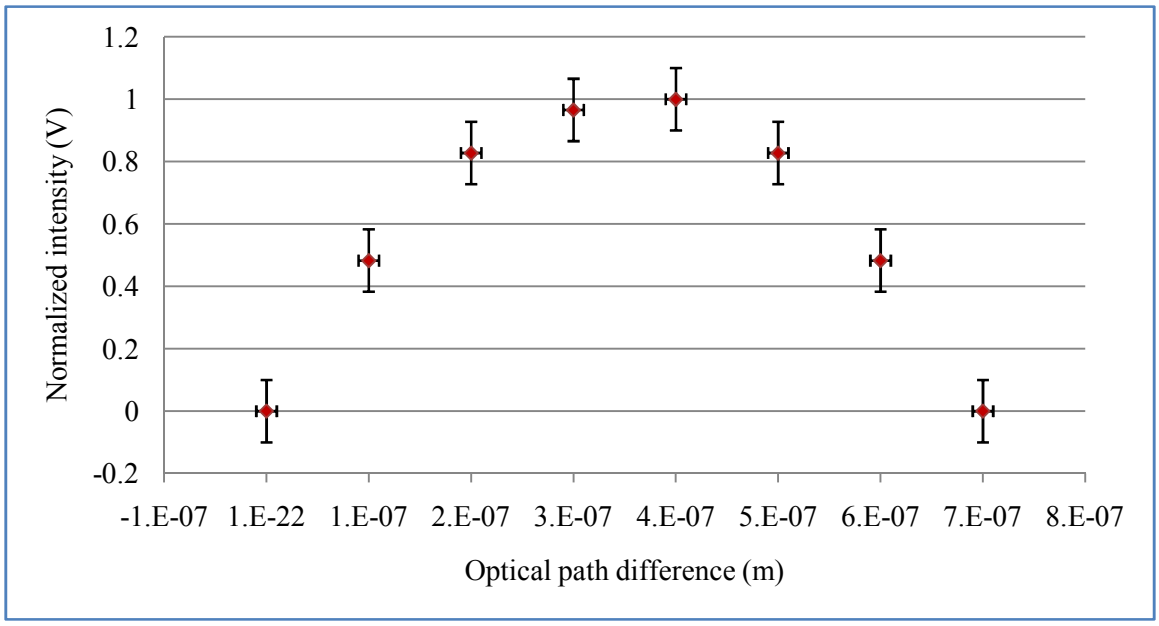

Figure 5.2 Experimental data for the distilled water sample.

The FWHM of the experimental data is 5.419×10^{-7}m. This value was substituted in Equation (4.17) to obtain the refractive index of water. The measured refractive index of the water sample, n_w, using this method is 1.35393. The same procedure was repeated a number of times in order to conduct an error analysis. Through error analysis, the standard deviation in the refractive index was calculated as 0.1. A high standard deviation was observed because of the difference in the FWHM of each data set, which resulted because, using the micrometer, it was only possible to change the path length difference in 100nm steps. This resulted in only seven data points for each data set.

Different kinds of motarized actuators with different resolutions were tested to move the traslation stage at the specified speed with a better resolution to get more data points. A piezo electric actuator (Burleigh) operated by a programmable ramp generator (RC-44, Burleigh) but it did not have the required step size and speed. Different kinds of actuators (Thorlabs) were tested with different ramp generators. Some actuators produced excessive vibration when they moved at the required speed, which affected the data. A high resolution actuator with a step size of approximately 25nm would have yielded more data points, thereby obtaining a better result with a low standard deviation. A few manufacturing companies provide the required actuators, but they are expensive.

For the fringe counting method, the liquid cell was translated manually with the micrometer to obtain a total path length difference of 1mm. The interference intensities were simultaneously recorded continuously using the image processing software. A sample picture of the data recording is shown in Figure 3.6. The total number of fringes in the 1mm path length difference was counted in two different ways: one way used the image processing software, and the other way counted the fringes manually by plotting the experimental data in a spreadsheet. The fringe-count data was then used in Equation (4.19) to calculate the refractive index of the water sample. The same procedure was repeated ten times and the standard deviation was calculated. The measured refractive index of the water, n_w, using the fringe-counting method was 1.331903, and the standard deviation was better than $1x10^{-6}$.

The refractive indices of different liquid samples were also measured. RP-1 (liquid rocket fuel) is a highly refined form of kerosene used as a rocket fuel. Although having a lower specific impulse than liquid hydrogen (LH_2), RP-1 is cheaper, can be

stored at room temperature, is far less of an explosive hazard and is far denser (0.81 g/ml). The measured refractive index of RP-1using this method was 1.454350, and the standard deviation was $1x10^{-6}$. Glycerin is a colorless, odorless, viscous liquid that is widely used in pharmaceutical formulations. In food and beverages, glycerin serves as a solvent and sweetener, and may help preserve foods. Glycerin has a density 1.261 g/cm^3. The measured refractive index of Glycerin using this method was 1.471436, and the standard deviation was $1x10^{-6}$. Alcohol absolute is commonly available in lab which works as a reaction agent, which has density of 0.783 g/cm^3. The measured refractive index of Alcohol using this method was 1.360696, and the standard deviation was $1x10^{-6}$.The measured refractive index of cooking oil (vegetable oil) using this method was 1.47460, and the standard deviation was $1x10^{-5}$. The refractive indices of these liquids are shown in Table 5.3.

Table 5.3 The refractive indices of different liquid samples.

Liquid	**Refractive Index (This work)**	**Refractive Index (Others)**
Water	$1.331903 \pm 1x10^{-6}$	1.330± 0.01(Leung & Vandiver)
RP-1 (liquid rocket fuel)	$1.454350 \pm 1x10^{-6}$	
Glycerin	$1.471436 \pm 1x10^{-6}$	1.472± 0.01
Alcohol (Ethyl Alcohol)	$1.360696 \pm 1x10^{-6}$	1.360± 0.01(Leung & Vandiver)
Cooking oil	$1.47460 \pm 1x10^{-6}$	1.47± 0.01

5.2 Measuring the Refractive Index of Sugar Solutions

The refractive indices of different concentrations of sugar solutions were measured using the fringe-counting method. Sugar and water were used in order to make 5%, 10%, 15%, 20%, and 25% sugar solutions. For example, a 5% sugar solution was made of 5gm of sugar and 95gm of water. The refractive index of each sugar solution was measured. A linear relationship between refractive index and the concentration has been observed by other researchers (W. Mahmood bin). The refractive indices of sugar solutions determined in the current work are shown in Table 5.4. A linear increase in the refractive index was observed when the density of the sugar solution increased. Figure 5.3 shows a plot of the percentage of sugar vs, the refractive index of the solution.

Table 5.4 The refractive indices of different concentrations of sugar solutions.

Concentration of the Sugar Solution	**Amount of Sugar (gm)**	**Amount of Water (gm)**	**Refractive Index of the Sugar Solution**
5%	5	95	$1.338548 \pm 1x10^{-6}$
10%	10	90	$1.341712 \pm 1x10^{-6}$
15%	15	85	$1.348040 \pm 1x10^{-6}$
20%	20	80	$1.354368 \pm 1x10^{-6}$
25%	25	75	$1.363860 \pm 1x10^{-6}$

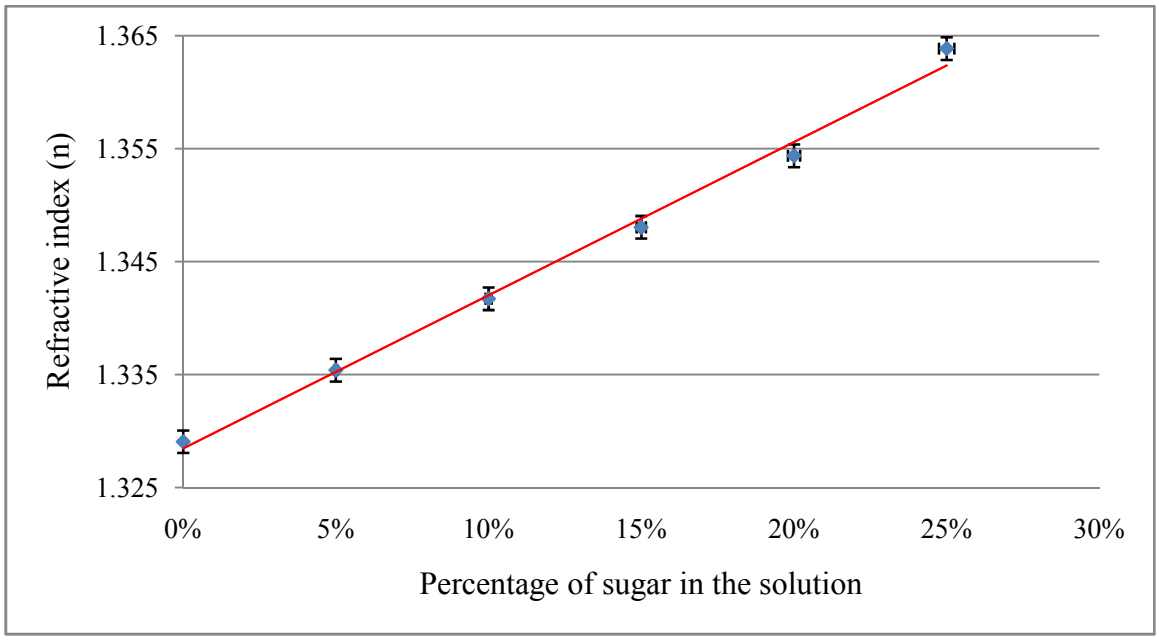

Figure 5.3 Percentage of sugar in the solution and the refractive index of the solution.

5.3 Error Analysis

An error analysis is required for any experimental investigation and this section describes the major sources of error seen in this research. Generally, there are two metrics used in describing an experimentally measured result: precision and accuracy. Although the two words can be synonymous in colloquial use, they are not the same thing in the scientific literature. In science and engineering, the accuracy of a measurement is an indication of how close an individual measurement is to the quantity's expected or accepted value. The precision of a measurement, referring to the reproducibility or repeatability, is the degree to which repeated measurements under identical conditions produce the same results.

Ideally a measurement device is both accurate and precise, with measurements all close to and tightly clustered around the expected value. A common convention in science and engineering is to express accuracy or precision through the number of significant digits given. In the fringe counting experiment, a manual micrometer with a minimum increment of 100nm was used to translate the liquid cell that changed the path length (Δl). Generally, the margin of the error using a scale is understood to be one-half of the finest measurable unit of that scale. Therefore, the error in the micrometer would be one-half of the minimum increment of the micrometer; that is ± 50 nm or 0.05 μm. The error in the path length difference would be Δl ± 50 nm (0.05 μm). If the wavelength 632.8 nm or 0.6328 μm of the laser source is assumed to have an error of ± 0.0001 μm, and fringes are counted in units of whole numbers with an error of ± 0.5 fringe and the total path length is 1 mm (1000 μm) with an error of 0.05 μm, a typical calculation for the index of refraction from Equation (4.19) would be

$$n_l = 1 + \frac{\lambda}{2}\frac{dm}{dL_l}$$

$$n_l = 1 + \left[\frac{0.6328 \pm 0.0001\mu m}{2}\right] x \left[\frac{950 \pm 0.5}{1000 \pm 0.05\mu m}\right],$$

where 950 is a typical value for the number of fringes counted in a 1 mm travel. Choosing the minimum extreme, the index is calculated to be 1.3004 and choosing the maximum the index is 1.3008, so for this example, the index would properly be stated as 1.3006+/-0.0002. This simple calculation is representative of those done throughout the research. It is interesting to note that even if the wavelength error is only +/- 0.00001 μm, the error in the index is the same. This illustrates the fact that while the precision of the

measurement in the present investigation may be limited by the number of significant digits the wavelength is known to, the accuracy of the index measurement is somewhat less.

The refractive index of liquids is also a function of temperature and pressure. A difference in temperature affects the density of the liquid, which in turn affects the refractive index. The change in the refractive index due to a temperature change is very small. Over each 10°C temperature change, the change in the refractive index of water is about $1x10^{-4}$ (Peck and Dobbins). In the present work, the temperature change was not more than 1°C. The index of refraction of liquids is also a function of pressure, but the dependence is quite weak because of the relative incompressibility. The approximate change in refractive index of water is 0.00001 when the pressure is increased by 1 atm (Quan and Fry). The refractive index of liquids was determined at room temperature and standard 1 atm pressure in this experiment.

CHAPTER 6

CONCLUSION

Since the refractive index is a fundamental physical property, it is often used to identify a particular substance, confirm its purity, or measure its concentration. The research presented in this thesis led to a method for determining the refractive index (n) of a given liquid accurately with low cost and minimum effort.

The refractive indices of a collection of liquids were measured using the FWHM method as well as the fringe-counting method using a modified interferometer. The main advantage of the modified interferometer was its simple experimental setup, which was built using inexpensive optical components that were available in the laboratory. The novel aspect of the research was the design and construction of a liquid cell that allowed accurate changes to be made in the optical path length. Image processing software was used to record, analyze, and accurately count the interference fringes.

The refractive indices of different liquids, including distilled water, RP-1 liquid rocket fuel, glycerin, absolute alcohol and vegetable oil, were all measured using this experimental technique. The refractive indices of different percentages of sugar solutions were also measured and the change in the refractive index with respect to the concentration of the sugar solution was determined.

Moving the translation stage more accurately would have provided an even more precise measurement of the index of refraction. An extensive search was done to determine the required actuator with better resolution which would also translate the liquid cell smoothly. Different kinds of actuators (850B for example) and motorized translation stages (ESP300 controller, Thorlabs) were tested during the investigation. Better actuators were found made by different companies. One is the PInano stage and controller (P-545 PInano, PIEZO NANO POSITIONING) having 200 μm travel with nanometer resolution. This stage is offered with adjustable speed and excellent stability. The other one is the Picometer actuator (8310, New Focus) and Picometer driver (8751, New Focus) having 12.7 mm travel range with minimum step size is less than 30 nm. These actuators can automate the experiment if the considerable expense can be justified.

APPENDIX

SIMULATION PROGRAM CODE

A Matlab program was written to simulate the plot of the normalized intensity (V) vs. optical path difference(Δl) (Figure 4.2).

```
clear all; clc
format long

R1 = 0.9;   %Reflectivity of the mirror mounted on PZT%
Rs = 0.9;   %Reflectivity of the sample%
Rm = 0.9;   %Reflectivity of the mirror M%
c = 3e8;    %speed of light%
dlamda = 25e-9;%spectral bandwidth%
L = [ ];
v = [ ];
V = [ ];
dpi=[ ];
delta=[ ];
index=[ ];
```

```
index1=[ ];

fwhm1=[ ];

lamda0=632.8e-9;   %central wavelenght in meter%

 lg=2.5e-3; %thickness of quartz window

     B1=0.696166300;% Sellemeier constants of quartz window%

    C1=4.67914826e-3;

    B2=0.407942600;

    C2=1.35120631e-2;

    B3=0.897479400;

    C3=97.9340025;

    %Sellemeier equation of the quartz window%

ng  =   (1+(B1*(lamda0/1e-6)^2/((lamda0/1e-6)^2-C1))+

          (B2*(lamda0/1e-6)^2/((lamda0/1e-6)^2-C2))+

          (B3*(lamda0/1e-6)^2/((lamda0/1e-6)^2-C3)))^0.5;


    D1=5.684027565e-1;%Sellemeier contants of water%

    D2=5.101829712E-3;

    D3=1.726177391E-1;

    D4=1.821153936E-2;

    D5=2.086189578E-2;

    D6=2.620722293E-2;

    D7=1.130748688E-1;

    D8=1.069792721E1;
```

```
    %Sellemeier equation of the water%
nw  =  (1+(D1*(lamda0/1e-6)^2/((lamda0/1e-6)^2-D2))+
          (D3*(lamda0/1e-6)^2/((lamda0/1e-6)^2-D4))+
          (D5*(lamda0/1e-6)^2/((lamda0/1e-6)^2-D6))+
          (D7*(lamda0/1e-6)^2/((lamda0/1e-6)^2-D8)))^0.5;
 clear L;
 clear V;
    L = [ ];
    v = [ ];
    V = [ ];
 for lw = -500e-9:28e-9:500e-9;
  L = [ L lw];
  P0=2e-3;%power of laser souece%
 gamma=.9;%quantum efficiency of photo detectors%
 WD = 60.32;        %doppler frequency in rad/s%
 w = 2*pi*c/lamda0;
 t = 0:.1:100;
 thita = 18*pi/180 ;
phip=((2*pi/lamda0)*(4.97e-6));
phis=((2*pi*2*lg*(1-ng)/lamda0)+(2*pi*2*lw*(1-nw)/lamda0)+
          (2*pi*(4.97e-6)/lamda0));
  deltaphi=(phis-phip);
  dpi=[dpi deltaphi];
```

```
Lp = WD*t+phip;

Ls = WD*t+phis;

Iw = (2*log(2)*lamda0^2)/(pi*dlamda);

Ip = max((gamma.*P0.*sqrt(R1*Rs)./2).*exp(-(2*lw.*sqrt(log(2))/Iw).^2).*cos(Lp));

Is = max((gamma*P0*sqrt(R1*Rm)/2).*exp(-(2*lw.*sqrt(log(2))/Iw).^2).*cos(Ls));

Idiff = max((gamma*P0*sqrt(R1)/2).*exp(-(2*lw.*sqrt(log(2))/Iw).^2)...

        .*sqrt(Rs+Rm-2*sqrt(Rs*Rm).*cos(deltaphi)).*cos(w*t-thita));

V = [V ((-Idiff.^2+Is.^2+Ip.^2)./(2.*Is.*Ip))];

 end

      V= V+1.3;

     V = V/max(V);

    LL= -600e-9:.01e-9:500e-9;

    VV= spline(L,V,LL);

    plot(LL,VV)

  x=LL;

 y=VV;

 y = y / max(y);

 N = length(y);



 [garbage,centerindex]=max(y) ;

 lev50 = garbage/2;

 i=centerindex;
```

```
if x(centerindex)>300e-9
        while y(i) > lev50
            i=i-1;
        end
    i=i+1;
else
        while y(i) > lev50
            i=i+1;

 end
    i=i-1;
   wid=(-1)*(2*(x(centerindex)-x(i)))
   fwhm1=[fwhm1 wid];
 index=[index lamda0];
 exportdata=[index',fwhm1'];
 exportdata1=[index1',fwhm1'];
%    xlswrite('lamdafwhmquartzwater.xls',exportdata);
%    xlswrite('indexfwhmquartzwater.xls',exportdata1);
 end
```

This Matlab program was written to measure the Full Width Half Maximum (FWHM) of the experimental data.

```
clear all; clc
format long

Data = xlsread('water714-1.xls');
L=Data(1:8,1);
V=Data(1:8,2);
        V= V-min(V);
        V = V/max(V);
    x= 0e-6:.001e-6:.7e-6;
     y= spline(L,V,x);

   plot(x,y)
   N = length(y);
  [garbage,centerindex]=max(y) ;
  lev50 = garbage/2;
  i=centerindex;
   if x(centerindex)>300e-9

  while y(i) > lev50
        i=i-1;
```

```
    end
     i=i+1;
     wid=(-1)*(2*(x(centerindex)-x(i)))
else
   while y(i) > lev50
       i=i+1;

    end
     i=i-1;
    wid=(-1)*(2*(x(centerindex)-x(i)))
end
```

REFERENCES

B. W. Grange, W. H. Stevenson and R. Viskanta, "Refractive index of liquid solutions at low temperature an accurate measurement," Appl. Opt, 858-859(1976).

P. Hariharan, "Optical Interferometry," Australia Academic Press, (1985).

C. Chou, H. Huang, and T. Hsieh, "Analog differential-phase detection in optical coherence reflectrometer," Opt. Exp, 12847-12858 (2008).

A. F. Leung and J. J. Vandiver, "Automatic refractometer," Opt. Eng, 1128-1131(2003).

M. Masumura and A. Daimon, "Measurement of the refractive index of distilled water from the near infrared region to the ultraviolet region," Appl. Opt, 3811-3820 (2007).

A. Suhadolnik, "An optical fiber interferometeric refractometer," Meas.Sci. Technol, 1205-1208 (2007).

C. Chou, J.C. Shyu, Y. C. Huang, and C. K. Yuan, "Common-path optical heterodyne profilometer a configuration," Appl. Opt, 4137-4142 (1998).

C. K. Hitzenberger and A. F. Fercher, "Differential phase contrast in optical coherence tomography," Opt.Lett, 622-624 (1999).

S. Yazdanfar and J. A. Izatt, "Self-referenced Doppler optical coherence tomography," Opt. Lett, 2085-2087 (2002).

C. Chou, C. W. Lyu, and L. C. Peng, "Polarized differential-phase laser scanning microscope," Appl. Opt, 96-99 (2001).

J. W. Goodman, "Introduction to Fourier Optics, 3rd ed.," Roberts and Company, Englewood, (2005).

D. P. Dave and T. E. Milner, "Optical low-coherence reflectometer for differential phase measurement," Opt. Lett, 227-229 (2000).

D. Huang, E. A. Swanson, C. P. Lin, J. S. Shuman, W. G. Stinson, W. Chang, M. R. Hee, T. Flottee, K. Gregory, C. A. Puliafito, and J. G. Fujimoto, “Optical coherence tomography,” Science, 1178-1181(1991).

E. Moreels, C. de Greef, and R. Finsy, “Laser light refractometer,” Appl. Opt, 3010 (1984).

M. V. R. K. Murty and R. P. Shukla, “Simple method for measuring the refractive index of a liquid,” Opt. Eng, 177–180 (1979).

M. V.R. K. Murty and R. P. Shukla, “Simple method for measuring the refractive index of a liquid or glass wedge,” Opt. Eng, 227–230 (1983).

W. Mahmood bin, Mat Yunus and Azizan bin Abdul Rahman, “Refractive index of solutions at high concentrations,” Appl. Opt, (1988).

H. M. Dobbins and E. R. Peck, “Change of refractive index of water as a function of temperature,” O.S.A(1973).

X. Quan and E. Fry, “Empirical equation for the index of refraction of seawater,” Appl. Opt, (1995).